DEVELOPMENT AND APPLICATION OF MASS TRANSFER CORRELATIONS FOR CO2 ABSORPTION IN PACKED COLUMNS

A Thesis

by

MATHEW T. DERICHSWEILER

Submitted to the Office of Graduate and Professional Studies of
Texas A&M University
in partial fulfillment of the requirements for the degree of

MASTER OF SCIENCE

Chair of Committee,	Mahmoud El-Halwagi
Committee Members,	Maria Barrufet
	Kenneth Hall
Head of Department,	Arul Jayaraman

December 2020

Major Subject: Chemical Engineering

ABSTRACT

A number of carbon capture and storage processes have been designed and implemented in an effort to mitigate the environmental impact of fossil fuel combustion in the energy industry. Since these processes can be retrofitted to existing plants, they offer a mechanism to reduce CO_2 emissions without phasing out of fossil fuel use. Of the carbon capture processes available, CO_2 absorption with alkanolamines, such as monoethanolamine or MEA, is perhaps the most widely used and viable. In many circumstances, random or structured packing is preferred over trays to provide ample surface area for gas-liquid contact while minimizing pressure drop inside the absorber column of a CO_2 absorption unit. However, packed columns are generally more difficult to model than trayed columns. The continuous nature of gas-liquid contact in packing makes rigorous mass transfer models more suitable than the vapor-liquid equilibrium (VLE) models commonly used for trayed columns. Despite the existence of many mass transfer correlations for packing in literature, no known set of correlations is accurate for the full range of available packing types, gas and liquid velocities, and gas/liquid system physical properties. This study seeks to develop a new set of mass transfer correlations useful for modeling CO_2 absorption in packed columns. A database of over 1300 values for effective interfacial mass transfer area (a_e) and the gas and liquid phase mass transfer coefficients (k_G and k_L) measured for both random and structured packings by the Process Science and Technology Center group at the University of Texas was consolidated and used to validate the correlations. The correlations for a_e, k_G, and k_L fit the database with average errors of 0.825%, 3.20%, and 7.14%, respectively. Predictions from the correlations were compared to those from other widely used literature correlations, and the new correlations were observed to better match the magnitudes and trends of data in the PSTC database. Finally, the correlations were incorporated into the process simulator ProMax and used to determine the optimal choice of packing on an economic basis to be used in a CO_2 absorber treating the flue gas from a 50MW coal-fired power plant.

ACKNOWLEDGMENTS

I would like to thank the members of my advisory committee, Dr. Mahmoud El-Halwagi, Dr. Maria Barrufet, and Dr. Ken Hall for their support and advice. I would also like to thank my coworkers at Bryan Research & Engineering. As a member of both groups, Dr. Ken Hall receives extra thanks. Dr. Jerry Bullin, Dr. Joel Cantrell, and Dr. Jorge Martinis have been excellent mentors, with Dr. Joel Cantrell being instrumental in helping me decide on a research topic. David Trettin and Steven Pan deserve thanks for their support and camaraderie.

I have to thank my parents for their support and encouragement throughout graduate school and all of the steps leading up to it in my life. Their love and belief in me has always kept me going.

Finally, I would like to thank Jaclyn Carpenter, Maggie, and Harry. I would not have been able to get to this point without their care, support, and reassurance at home.

CONTRIBUTORS AND FUNDING SOURCES

Contributors

This work was supported by a thesis committee consisting of Professor Mahmoud El-Halwagi and Dr. Kenneth Hall of the Department of Chemical Engineering and Professor Maria Barrufet of the Department of Petroleum Engineering. All work conducted for the thesis was completed by the student independently.

Funding Sources

There are no outside funding contributors to acknowledge related to the research and compilation of this document.

NOMENCLATURE

a_e	Effective interfacial mass transfer area (m^2/m^3)
a_p	Specific area of packing (m^2/m^3)
B	Corrugation base in structured packing (m)
C_A	Simple annualized cost ($/s)
$C_{absorber}$	Absorber purchase cost ($)
C_{blower}	Blower purchase cost ($)
C_{elec}	Electricity cost for blower ($/s)
C_E	Correction factor for surface renewal in Rocha, Bravo, and Fair mass transfer correlations
C_M	Material factor in developed mass transfer area correlation
C_{PK}	Packing cost ($/m^3)
Ca_L	Liquid-phase capillary number
c_G	Gas-phase molar density (kmol/m^3)
c_L	Liquid-phase molar density (kmol/m^3)
D_G	Gas-phase diffusion coefficient (m^2/s)
D_L	Liquid-phase diffusion coefficient (m^2/s)
d_c	Column diameter (m)
d_h	Hydraulic diameter (m)
d_p	Random packing size (m)
E	Enhancement factor for liquid-phase mass transfer coefficient in systems with chemical reactions
F_M	Material cost factor
Fr_L	Liquid-phase Froude number

F_{SE}	Surface enhancement factor in Rocha, Bravo, and Fair mass transfer correlations
G	Gas-phase molar flow rate (kmol/s)
g	Acceleration due to gravity (m/s^2)
g_{eff}	Effective acceleration due to gravity in Rocha, Bravo, and Fair mass transfer correlations (m/s^2)
H_A	Henry's law constant for component A (Pa)
h	Corrugation height in structured packing (m)
h_L	Liquid holdup
K_{OG}	Overall gas-phase mass transfer coefficient (m/s)
K_{OL}	Overall liquid-phase mass transfer coefficient (m/s)
k_G	Gas-phase mass transfer coefficient (m/s)
k_L	Liquid-phase mass transfer coefficient (m/s)
k_{OH^-}	CO_2-NaOH reaction rate constant (m^3/kmol s)
L	Liquid-phase molar flow rate (kmol/s)
l_τ	Length of flow path in Billet and Schultes mass transfer correlations (m)
N_A	Mass transfer flux of component A (kmol/s)
P	Pressure (Pa)
P_B	Blower power (W)
P_d	Column design pressure (Pa)
P_{stress}	Maximum allowable column stress (Pa)
ΔP_d	Dry pressure drop (Pa)
R	Ideal gas constant (kJ/kmol K)
Re_G	Gas-phase Reynolds number
Re_L	Liquid-phase Reynolds number
S	Side dimension of corrugation in structured packing (m)

Sc_G	Gas-phase Schmidt number
Sc_L	Liquid-phase Schmidt number
Sh_G	Gas-phase Sherwood number
T	Temperature (K)
t_s	Column shell thickness (m)
u_G	Gas-phase superficial velocity (m/s)
u_{Ge}	Gas-phase effective velocity (m/s)
u_L	Liquid-phase superficial velocity (m/s)
u_{Le}	Liquid-phase effective velocity (m/s)
V_{PK}	Packing volume (m^3)
W	Column weight (kg)
We_L	Liquid-phase Weber number
x_A	Liquid-phase mole fraction of component A (mol/mol)
x_A^i	Liquid-phase mole fraction of component A at gas-liquid interface (mol/mol)
x_A^*	Equilibrium liquid-phase mole fraction of component A (mol/mol)
$x_{A,in}$	Liquid-phase mole fraction of component A entering column (mol/mol)
$x_{A,out}$	Liquid-phase mole fraction of component A exiting column (mol/mol)
y_A	Gas-phase mole fraction of component A (mol/mol)
y_A^i	Gas-phase mole fraction of component A at gas-liquid interface(mol/mol)
y_A^*	Equilibruim gas-phase mole fraction of component A (mol/mol)
$y_{A,in}$	Gas-phase mole fraction of component A entering column (mol/mol)

$y_{A,out}$	Gas-phase mole fraction of component A exiting column (mol/mol)
Z	Height of packing (m)

Greek Letters

α	Corrugation angle in structured packing (°)
γ	Contact angle in Rocha, Bravo, and Fair mass transfer correlations (°)
$\delta_{Nusselt}$	Nusselt film thickness (m)
ε	Void fraction of packing
μ_G	Gas-phase dynamic viscosity (Pa s)
μ_L	Liquid-phase dynamic viscosity (Pa s)
ρ_G	Gas-phase density (kg/m^3)
ρ_L	Liquid-phase density (kg/m^3)
ρ_M	Column shell material of construction density (kg/m^3)
σ	Surface tension (N/m)
σ_c	Critical surface tension in Onda mass transfer correlations (N/m)

TABLE OF CONTENTS

Page

LIST OF FIGURES

FIGURE Page

LIST OF TABLES

TABLE Page

1. INTRODUCTION

1.1 Climate Change and CO_2 Absorption

Concern for anthropogenic climate change has prompted efforts to reduce the environmental impact of the energy industry. Generation of electrical power is still largely dependent on fossil fuel use, and fossil fuel use is the most common source of greenhouse gas emissions, mainly in the form of CO_2 released post-combustion [EIA, 2020]. In the United States, combustion of fossil fuels accounts for approximately 63% of electricity produced [EPA, 2018]. As a result, 27% of all 2018 US greenhouse gas emissions could be attributed to electricity production. Complete phasing out of fossil fuel combustion in the near future is unlikely given its prevalence, so reduction of greenhouse gas emissions from existing combustion processes is an important target for climate change mitigation.

Carbon capture and storage technologies are a family of processes that separate CO_2 from gas mixtures and dispose of it without venting to the atmosphere. When retrofitted to flue gas streams in power plants, they offer a way to reduce CO_2 emissions from fossil fuel combustion. Several technologies have been developed for this purpose, including absorption, adsorption, cryogenic distillation, and membrane processes [Rao and Rubin, 2002]. Among these, absorption is considered to be the most generally well-suited and feasible for several reasons. First, absorption processes are effective for feed streams with dilute CO_2 concentrations. This is important for carbon capture processes because flue gases from coal and natural gas plants are often less than 12% CO_2 by volume. Second, absorption processes are already widely used in industry. They are the standard technology for many gas treating applications, such as acid gas removal from natural gas, tail gas treating in sulfur recovery units, and CO_2 removal from syngas in ammonia production. Third, they can be easily scaled. The main unit operations used in absorption are staged columns, heat exchangers, and pumps, which are all commercially available in a variety of sizes. Finally, absorption processes can be operated at relatively mild conditions. Temperatures typically range

from ambient to 120°C, and pressures typically range from atmospheric to 250 kPa. As a result, absorption processes incur moderately low equipment costs, utility costs, and safety risks compared to other carbon capture technologies.

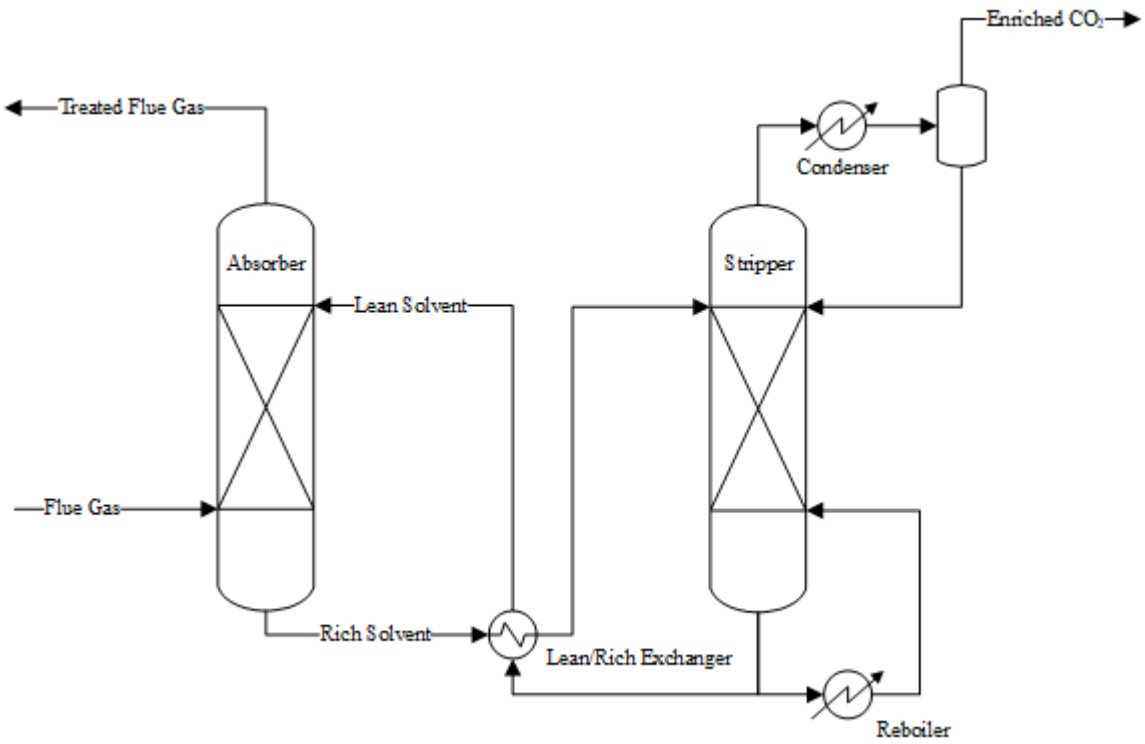

Figure 1.1: Process flow diagram for a generic CO_2 absorption process.

A generalized absorption process is shown in Figure 1.1. The flue gas feed stream enters the bottom of a staged column, typically referred to as the absorber or contactor. Here, the flue gas is brought into contact with a liquid solvent via countercurrent flow across the column internals. CO_2 gets absorbed by the solvent physically or through a chemical reaction, and the treated flue gas exits the top of the absorber. The rich solvent exits the bottom of the absorber and is sent to the top of a second staged column called the stripper or regenerator. The absorbed CO_2 reenters the vapor phase as the solvent flows down the column internals and exits the top of the stripper. A partial condenser helps to further enrich the CO_2 product stream and provide reflux. The lean solvent exits

the bottom of the stripper and is recycled back to the absorber. A reboiler vaporizes a portion of the lean solvent stream to provide heat for the CO_2-solvent separation. Usually, a heat exchanger is installed to transfer heat from the lean solvent to the rich solvent, which simultaneously makes CO_2 absorption more favorable in the lean solvent and CO_2 desorption more favorable in the rich solvent.

Many physical and chemical solvents have been developed for use in CO_2 absorption units. Among chemical solvents, solutions of alkanolamines in water are the most common. Alkanolamines are a class of compounds with the generic formula $NR_1R_2R_3$, where at least one of the substituents R_1, R_2, or R_3 is an alcohol. Because of the lone electron pair on the nitrogen atom, they function as weak bases. Since CO_2 forms carbonic acid in the presence of water, alkanolamines provide a chemical gradient for CO_2 absorption in aqueous solutions. The main reactions that occur in the liquid phase of a system with CO_2, water, and a primary alkanolamine (NH_2R) are shown below.

$$CO_2 + H_2O \longleftrightarrow H^+ + HCO_3^-$$

$$CO_2 + NH_2R \longleftrightarrow H^+ + HNRCOO^-$$

$$H^+ + NH_2R \longleftrightarrow NH_3R^+$$

The second reaction can only occur when at least one of the substituents on the nitrogen atom is a hydrogen atom. This makes CO_2 absorption more favorable in primary alkanolamines and secondary alkanolamines (NHR_1R_2) than in tertiary alkanolamines ($NR_1R_2R_3$). One of the most popular alkanolamines used for CO_2 absorption is monoethanolamine (MEA), a primary alkanolamine. MEA is very reactive compared to other alkanolamines, making it effective even at low pressures and flue gas CO_2 concentrations. However, it is also very corrosive. To avoid equipment degradation, MEA concentration in the lean solvent is usually kept below 30 wt%, and solvent flow rates are adjusted to keep rich loading below 0.35 mol CO_2/mol MEA [BRE, 2020a].

1.2 Packed Columns

Trays or packing may be used as column internals for the absorber and stripper in a CO_2 absorption unit. The choice of which type of internals to use has significant implications for unit performance, capital cost, and maintenance. Generally, the objective is to maximize the surface area available for gas-liquid contact inside the column while minimizing pressure drop and issues associated with installation and upkeep. In terms of these goals, packing can offer several advantages over trays [Towler and Sinnott, 2013]. First, packing typically incurs a lower pressure drop than trays. This is a significant advantage in CO_2 capture applications, where the flue gas feed often exits the power plant near atmospheric pressure. Second, packing is easier to install and maintain in columns with a small diameter. Because of this, packed columns can be designed for a wider range of scales. Third, packing typically offers a lower liquid holdup. Reducing liquid holdup improves safety and can decreases the rate of equipment degradation in systems with caustic liquids, such as MEA. Finally, packing is associated with a lower tendency for foaming, which can both reduce gas-liquid contact area and increase pressure drop.

1.2.1 Random Packing

Random, or dumped, packing is a type of packing that consists of numerous small individual objects dumped into a column shell. The objects settle into a random configuration inside the column, forming a loosely-packed bed. Some examples of different types of random packing are shown in Figure 1.2. One of the oldest and perhaps simplest types of random packing is the Raschig ring, which is merely an annular cylinder. Objects with more complex geometries that offer more surface area for gas-liquid contact and better fluid flow distribution have since been developed. Generally, a given type of random packing is available in a variety of sizes and materials of construction, such as metal, ceramic, and plastic. Random packings are quantitatively defined by their specific area (a_p), void fraction (ε), and nominal packing size (d_p).

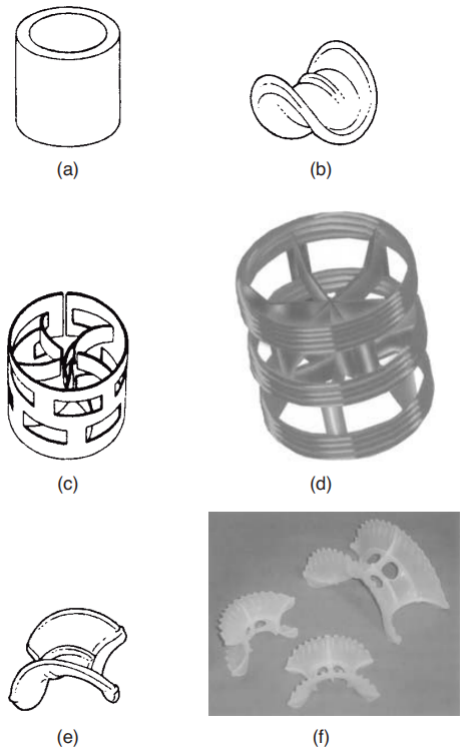

Figure 1.2: Examples of different types of random packing. (a) Raschig ring. (b) Berl saddle. (c) and (d) Pall ring. (e) Intalox saddle. (f) Super Intalox saddle. Reprinted from [Green and Perry, 2008]

1.2.2 Structured Packing

Structured packing is a type of packing that consists of large pre-constructed units containing layers of corrugated sheets or wire mesh with identical geometry. The units are carefully arranged and stacked in the column shell. An example of structured packing with corrugated sheets is shown in Figure 1.3. Structured packing types are differentiated by the dimensions of their corrugated sheets and the angle at which they are arranged. The relevant dimensions are the corrugation base (B), corrugation height (h), corrugation side (S), and corrugation angle (α). A diagram displaying these dimension is shown in Figure 1.4. Like random packing, structured packing is typically available in metal, ceramic, and plastic forms. The specific area and void fraction parameters are also used to characterize structured packing.

An absorber or stripper may use either random or structured packing. Structured packing usu-

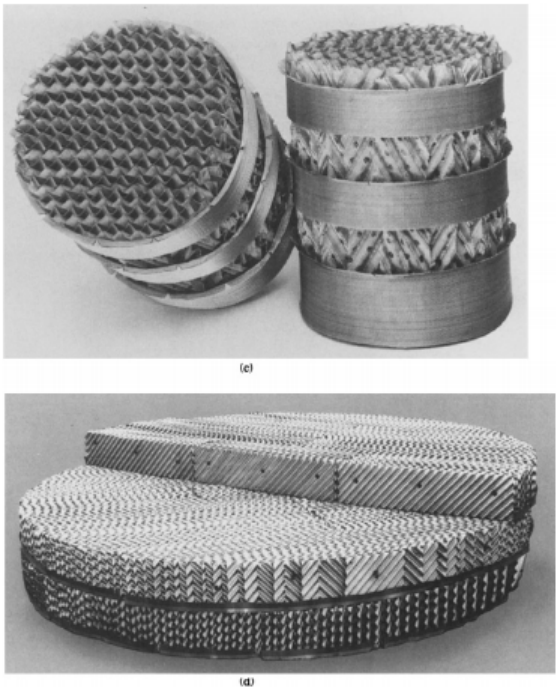

Figure 1.3: Examples of structured packing. Reprinted from [Kister, 1992]

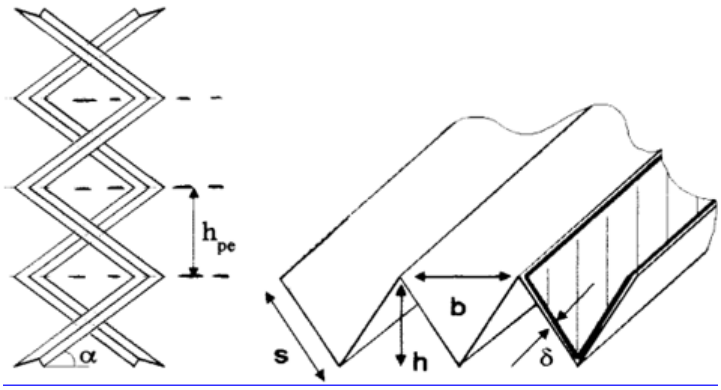

Figure 1.4: Diagram of structured packing dimensions. Reprinted from [Olujic et al., 2001]

ally offers more surface area per volume of packing [Green and Perry, 2008]. This means structured packing allows for more gas-liquid contact and therefore greater performance. Structured packing also tends to be associated with a lower pressure drop than random packing. However, random packing tends to be less expensive than structured packing. Additionally, the performance advantage of structured packing over random packing decreases at low liquid flow rates.

1.3 Mass Transfer Modeling

Rigorous modeling of the absorber and stripper in a CO_2 absorption unit is important for proper design. Overestimation of the performance of either column can result in a unit that is unable to meet targeted CO_2 concentration specifications in the treated flue gas, while underestimation can result in excess capital costs. In a column with random or structured packing, gas-liquid contact occurs continuously throughout the height of the packing. This differs from a column with trays, in which gas-liquid contact is mostly confined to the surface of each tray. A vapor-liquid equilibrium (VLE) model, which assumes the gas and liquid are in equilibrium a finite number of times in the column, is therefore more appropriate for a trayed column than a packed column. A mass transfer model, which considers continuous interchange of components between the gas and liquid phases, is more appropriate than a VLE model for packed columns [Skowlund et al., 2012].

Mass transfer models are based on the material balance around a differential cross-sectional element of the column. An illustration of this is given in Figure 1.5. For an element of height dh

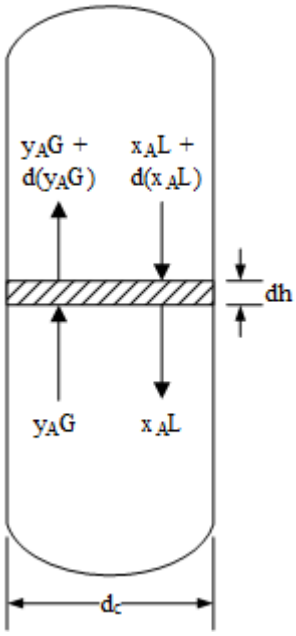

Figure 1.5: Material balance on a differential element of a packed column.

inside the column, the material balance for component A in the gas phase is given in Equation 1.1.

$$-d(y_A G) = N_A a_e \pi \left(\frac{d_c}{2}\right)^2 dh \tag{1.1}$$

Here, N_A is the mass transfer flux of component A from the gas phase to the liquid phase and a_e is the effective interfacial mass transfer area. N_A can be represented in a variety of ways. The most useful representation for the calculation of concentration profiles in a column is given in Equation 1.2,

$$N_A = K_{OG} c_G (y_A - y_A^*) \tag{1.2}$$

where K_{OG} is the overall gas phase mass transfer coefficient and y_A^* is the equilibrium mole fraction of component A in the gas phase. K_{OG} can be calculated by considering the other ways N_A can be represented. Due to conservation of mass, the mass transfer flux of component A from the gas phase to the liquid phase is equal to the mass transfer flux of component A from the bulk gas phase to the gas-liquid interface (Equation 1.3) and from the gas-liquid interface to the bulk liquid phase (Equation 1.4).

$$N_A = k_G c_G (y_A - y_A^i) \tag{1.3}$$

$$N_A = k_L c_L (x_A^i - x_A) \tag{1.4}$$

k_G and k_L are the gas and liquid phase mass transfer coefficients, respectively, which govern mass transfer from the bulk phase to the phase interface. y_A^i and x_A^i are the gas and liquid phase mole fractions at the gas-liquid interface, respectively. From these equations for N_A, the inverse of the overall gas phase mass transfer coefficient can be expressed as Equation 1.5.

$$\frac{1}{K_{OG}} = \frac{1}{k_G} + \frac{1}{k_L}\frac{c_G}{c_L}\frac{y_A^i - y_A^*}{x_A^i - x_A} \tag{1.5}$$

Assuming component A is dilute in the liquid phase, Equation 1.5 can be simplified to Equation

1.6

$$\frac{1}{K_{OG}} = \frac{1}{k_G} + \frac{1}{k_L}\frac{c_G}{c_L}\frac{H_A}{P} \tag{1.6}$$

where H_A is the Henry's law constant for component A.

Equations 1.1, 1.2, and 1.6 are useful for modeling the absorber or stripper in a CO_2 absorption unit when a physical solvent is used. When a chemical solvent, such as MEA, is used, the liquid phase mass transfer coefficient must be multiplied by an enhancement factor to account for the chemical reaction that occurs in the liquid phase. Equation 1.6 then becomes

$$\frac{1}{K_{OG}} = \frac{1}{k_G} + \frac{1}{Ek_L}\frac{c_G}{c_L}\frac{H_A}{P} \tag{1.7}$$

where E is the enhancement factor. In this case, k_L only describes the mass transfer that drives physical absorption of component A, and E has a value greater than or equal to 1 to account for the increase in mass transfer rate caused by the reaction. The expression for E depends on the rate expression for the chemical reaction.

k_G, k_L, and a_e must be known to calculate the mass transfer flux of a component from the gas phase to the liquid phase. These parameters are usually calculated using correlations from mechanistic, empirical, or semi-empirical models. When empirical or semi-empirical models are used, the parameters are typically defined via dimensionless expressions to allow for scaling. a_e is calculated in terms of a_e/a_p, where a_p is the specific area, or surface area per unit volume, of the packing. k_G and k_L may be calculated in terms of the Sherwood number, which is a dimensionless representation of the concentration gradient at the gas-liquid interface. For the gas phase, the Sherwood number is expressed as Equation 1.8.

$$Sh_G = \frac{k_G d_h}{D_G} \tag{1.8}$$

$$Sh_{G/L} = \frac{k_{G/L} d_h}{D_{G/L}} \tag{1.9}$$

$$Sc_{G/L} = \frac{\mu_{G/L}}{\rho_{G/L} D_{G/L}} \tag{1.10}$$

The liquid phase Sherwood number (Sh_L) is expressed similarly, but with k_G and D_G substituted for the analogous liquid phase parameters. The hydraulic diameter, d_h, is a characteristic length measurement that often has different definitions across different models. Other dimensionless parameters commonly found in correlations for a_e, k_G, and k_L include the Reynolds number, Schmidt number, Froude number, and Weber number. Like the Sherwood number, they can be defined for either the gas phase or the liquid phase with analogous expressions. Equations 1.11-1.14 give the definitions for the liquid phase.

$$Re_L = \frac{\rho_L u_L d_h}{\mu_L} \tag{1.11}$$

$$Sc_L = \frac{\mu_L}{\rho_L D_L} \tag{1.12}$$

$$Fr_L = \frac{u_L^2}{g d_h} \tag{1.13}$$

$$We_L = \frac{u_L^2 \rho_L d_h}{\sigma} \tag{1.14}$$

The Reynolds number (Equation 1.11) represents the ratio of inertial to viscous forces in fluid flow [Incropera et al., 2007]. The Schmidt number (Equation 1.12) represents the ratio of momentum to mass diffusivity. The Froude number (Equation 1.13) represents the ratio of inertial to gravitational forces. Finally, the Weber number (Equation 1.14) represents the ratio of inertial to surface tension forces. Developers of mass transfer correlations often utilize some combination of these dimensionless numbers to indicate the driving forces governing mass transfer. The relative importance of each driving force can be expressed by regressing exponents for each number in the correlation.

2. LITERATURE REVIEW

2.1 Mass Transfer Correlations

Many correlations for gas and liquid phase mass transfer coefficients and effective interfacial mass transfer area in packed columns have been developed. These correlations differ in the types of packings for which they are applicable and the range of operating conditions for which they are accurate. The help files included in the process simulator ProMax give a good overview of the applicability and limitations of each correlation included in the software. Tables 2.1-2.3 list the correlations that will be reviewed in this work along with the systems and packings that were used to develop them [BRE, 2020b].

Author	Gas/Liquid Systems Used to Develop Correlation
Onda et al. (1968)	CO_2/Water, CO_2/CCl_4, CO_2/Methanol, Air/Water, Benzene-Toluene-Methanol/Water, Ethanol/Water
Bravo and Fair (1982)	Cyclohexane/n-Heptane, n-Butane/Isobutene, 1-Propanol/Water, Ethylbenzene/Styrene, Methanol/Ethanol, Ethanol/Water, n-Heptane/Toluene, Benzene/Dichloroethane, Isooctane/Toluene, NH_3-Air/Water, O_2-Air/Water
Billet and Schultes (1993)	CO_2/Water, CO_2/Methanol, CO_2/Aqueous Salt Solutions, Cl_2-Air/Water, Air/Methanol, Air/Benzene, Helium/Water, Freon-12/Water, NH_3-N_2/Water, NH_3-Propane/Water, SO_2-Air/Water, Acetone-Air/Water, Ethanol-Air/Water, Chlorobenzene/Ethylbenzene, Toluene/n-Octane, Ethanol/Water, Ethylbenzene/Styrene, Methanol/Ethanol, 1,2-Dichloroethane/Toluene
Rocha, Bravo, and Fair (1996)	Air/Water, Cyclohexane/n-Heptane, Ethylbenzene/Styrene, Methanol/Ethanol, Chlorobenzene/Ethylbenzene, i-Butane/n-Butane
Hanley and Chen (2012)	Hexane/n-Heptane, 1,2-Propylene Glycol/Ethylene Glycol, Ethylbenzene/Styrene, i-Propane/n-Propane, i-Octane/Toluene, D_2O/Water, Chlorobenzene/Ethylbenzene, p-Xylene/o-Xylene, Argon/Oxygen, CO_2/Aqueous MEA, CO_2/Aqueous AMP

Table 2.1: Systems used in literature mass transfer correlations.

Author	Random Packings Used to Develop Correlation
Onda et al. (1968)	Raschig Rings, Berl Saddles, Spheres, Rods
Bravo and Fair (1982)	Berl Saddles, Raschig Rings, Pall Rings
Billet and Schultes (1993)	Pall Rings, Ralu Rings, NOR PAC Rings, Hiflow Rings, TOP-Pac Rings, Raschig Rings, VSP Rings, Envi Pac Rings, Bialecki Rings, Tellerettes, Spheres, Berl Saddles, Intalox Saddles
Rocha, Bravo, and Fair (1996)	N/A
Hanley and Chen (2012)	IMTP, Pall Rings, Nutter Rings

Table 2.2: Random packings used in literature mass transfer correlations.

Author	Structured Packings Used to Develop Correlation
Onda et al. (1968)	N/A
Bravo and Fair (1982)	N/A
Billet and Schultes (1993)	Ralu Pack YC-250, 250; Impulse Packing 50-100; Montz Packing B1-200, B1-300, C1-200, C2-200; Euroform PN-110
Rocha, Bravo, and Fair (1996)	FLEXIPAC 2; GEMPAK 2A, 2AT; Intalox 2T; MaxPak; Mellapak 250Y, 350Y, 500Y; Sulzer BX
Hanley and Chen (2012)	Intalox 2T; FLEXIPAC 500Y; Mellapak 250Y, 750Y; Koch-Glitsch BX, DX, EX

Table 2.3: Structured packings used in literature mass transfer correlations.

Onda et al. developed one of the first widely used set of correlations for mass transfer in packed columns [Onda et al., 1968]. The correlations, given in Equations 2.1-2.3, utilize empirical relationships for both mass transfer coefficients and interfacial area.

$$Sh_G = 5.23 Re_G^{0.7} Sc_G^{1/3} (a_p d_p)^{-2.0} \tag{2.1}$$

$$k_L \left(\frac{\rho_L}{\mu_L g}\right)^{1/3} = 0.0051 \left(\frac{\rho_L u_L}{a_e \mu_L}\right)^{2/3} Sc_L^{-1/2} (a_p d_p)^{0.4} \tag{2.2}$$

$$\frac{a_e}{a_p} = 1 - exp\left[-1.45 \left(\frac{\sigma_C}{\sigma}\right)^{0.75} Re_L^{0.1} Fr_L^{-0.05} We_L^{0.2}\right] \tag{2.3}$$

The hydraulic diameter used in calculating Sh_G, Re_G, Re_L, Fr_L, and We_L is defined as $d_h = 1/a_p$ in this context. σ_c is the critical surface tension, which is a property of packing material of

construction. Values of σ_c for the materials of construction used in developing the correlations are given in Table 2.4 [Towler and Sinnott, 2013]. The correlations fit the data used to validate

Packing Material of Construction	σ_c (mN/m)
Ceramic	61
Metal (steel)	75
Plastic (polyethylene)	33
Carbon	56

Table 2.4: Critical surface tension values for common packing materials.

them within ±20% for absorption cases and ±30% for distillation cases. However, the correlations were not validated with data from structured packings and therefore are only applicable to random packings. Furthermore, the random packings used by Onda et al. were early-developed packings with simple geometries. The correlations preceded the development of modern random packings with more complex geometries. Another limitation of the Onda correlations is the upper-limit of 1 imposed on a_e/a_p by the form of Equation 2.3. This upper-limit assumes that the effective interfacial mass transfer area cannot be greater than the total surface area of the packing. Since the descending liquid phase in a packed column can form droplets and waves that provide additional gas-liquid contact area, this assumption is not necessarily true.

Bravo and Fair further developed the Onda correlations to produce another widely used set of mass transfer correlations for random packing [Bravo and Fair, 1982]. They left the correlations for the gas and liquid phase mass transfer coefficients unaltered, but they developed the following correlation for the effective interfacial mass transfer area:

$$\frac{a_e}{a_p} = 0.498 \left(\frac{\sigma(\text{dyn/cm})^{0.4}}{Z(\text{ft})^{0.5}} \right) (6Ca_L Re_G)^{0.392} \tag{2.4}$$

Ca_L is the liquid phase capillary number, which is the liquid phase Weber number divided by the liquid phase Reynolds number ($Ca_L = We_L/Re_L$). This correlation for a_e/a_p removed the upper-

limit of 1 imposed by the Onda correlations. However, the range of packing types used to validate the correlation was still somewhat narrow and excluded structured packings.

Billet and Schultes developed a set of mass transfer correlations validated with a large number of gas-liquid systems, random packings, and structured packings [Billet and Schultes, 1993]. The expressions for the gas and liquid phase mass transfer coefficients are based on a fundamental model for mass transfer called penetration theory, making them somewhat mechanistic. The Billet and Schultes correlations are given in Equations 2.5-2.7.

$$k_G = C_G \frac{1}{(\varepsilon - h_L)^{1/2}} \frac{D_G a_p^{1/2}}{l_\tau^{1/2}} \left(\frac{\rho_G u_G}{a_p \mu_G} \right)^{3/4} Sc_G^{1/3} \tag{2.5}$$

$$k_L = C_L \left(\frac{\rho_L g}{\mu_L} \right)^{1/6} \left(\frac{D_L}{l_\tau} \right)^{1/2} \left(\frac{u_L}{a_p} \right)^{1/3} \tag{2.6}$$

$$\frac{a_e}{a_p} = 1.5 \left(a_p l_\tau \right)^{-0.5} Re_L^{-0.2} We_L^{0.75} Fr_L^{-0.45} \tag{2.7}$$

C_G and C_L are dimensionless constants that were regressed for various random and structured packings. l_τ is the length of the flow path in penetration theory. In this context, it is equal to the hydraulic diameter used in calculating Re_L, We_L, and Fr_L. Billet and Schultes used the following definition:

$$l_\tau = d_h = 4 \frac{\varepsilon}{a_p} \tag{2.8}$$

The correlation for k_G also used liquid holdup, h_L, which was calculated with Equation 2.9.

$$h_L = \left(12 \frac{1}{g} \frac{\mu_L}{\rho_L} u_L a_p^2 \right)^{1/3} \tag{2.9}$$

The Billet and Schultes correlations were particularly useful because they were validated for both random and structured packings. Furthermore, the introduction of the packing-specific constants C_G and C_L provided a mechanism to address magnitude inaccuracies in applying the correlations to packings not validated in the study. However, C_G and C_L must be determined experimentally for each packing used with the correlations. Additionally, many popular modern random

and structured packings, such as IMTP and the Sulzer Mellapak series, were not used in the development of the form of the correlation equations.

Rocha, Bravo, and Fair developed a separate set of correlations that were also inspired by penetration theory [Rocha et al., 1996]. The liquid phase mass transfer coefficient correlation (Equation 2.11) utilized the mechanistic model, while the correlations for the gas phase mass transfer coefficient (Equation 2.10) and effective interfacial area (Equation 2.12) utilized empirical relationships.

$$Sh_G = 0.054 \left(\frac{(u_{Ge} + u_{Le})\, \rho_G S}{\mu_G} \right)^{0.8} Sc_G^{0.33} \tag{2.10}$$

$$k_L = 2 \left(\frac{D_L C_E u_{Le}}{\pi S} \right)^{1/2} \tag{2.11}$$

$$\frac{a_e}{a_p} = F_{SE} \frac{29.12 \left(We_L Fr_L\right)^{0.15} S^{0.359}}{Re_L^{0.2} \varepsilon^{0.6} \left(1 - 0.93 \cos\gamma\right) \left(\sin\alpha\right)^{0.3}} \tag{2.12}$$

C_E and F_{SE} are dimensionless constants used to account for imperfect surface renewal by the liquid phase and surface enhancement features present in the packing, respectively. Rocha, Bravo, and Fair assumed a value of 0.9 for C_E, and F_{SE} is a property of the type of packing used. S is the side length of the corrugation in corrugated sheet structured packing. The hydraulic diameter d_h used in calculating Re_L, Fr_L, and We_L is taken to be equal to S. α is the corrugation angle, or the angle at which the corrugated sheets in a bundle of structured packing are arranged. γ is defined as the contact angle, which is taken to be a function of surface tension:

$$\cos\gamma = \begin{cases} 0.9 & \sigma \leq 0.055 N/m \\ 5.211 \times 10^{-16.835\sigma} & \sigma > 0.055 N/m \end{cases} \tag{2.13}$$

The correlations for the mass transfer coefficients use effective velocities for the gas and liquid phases (u_{Ge} and u_{Le}, respectively) rather than superficial velocities. These are given by the following expressions:

$$u_{Ge} = \frac{u_G}{\varepsilon \left(1 - h_L\right) \sin\alpha} \tag{2.14}$$

$$u_{Le} = \frac{u_L}{\varepsilon h_L \sin\alpha} \tag{2.15}$$

Like the Billet and Schultes correlations, the Rocha, Bravo, and Fair correlations assume the mass transfer coefficients have a dependence on liquid holdup. However, Rocha, Bravo, and Fair used a different correlation to calculate liquid holdup:

$$h_L = \left(4\frac{1}{F_{SE}S}\frac{a_e}{a_p}\right)^{2/3}\left(\frac{3\mu_L u_L}{\rho_L g_{eff}\varepsilon\sin\alpha}\right)^{1/3} \tag{2.16}$$

$$g_{eff} = g\frac{\rho_L - \rho_G}{\rho_L}\left(1 - \frac{\Delta P/\Delta Z}{1025}\right) \tag{2.17}$$

$$\frac{\Delta P}{\Delta Z} = \frac{\Delta P_d}{\Delta Z}\left[\frac{1}{1-(0.614+71.35S)\,h_L}\right]^5 \tag{2.18}$$

$$\frac{\Delta P_d}{\Delta Z} = \frac{0.177\rho_G}{S\varepsilon^2\left(\sin\alpha\right)^2}u_G^2 + \frac{88.774\mu_G}{S^2\varepsilon\sin\alpha}u_G \tag{2.19}$$

Equations 2.16-2.19 must be solved for h_L and $\Delta P/\Delta Z$. This can be done via iterative substitution with an initial guess of $\Delta P/\Delta Z = \Delta P_d/\Delta Z$.

The Rocha, Bravo, and Fair correlations provided a more rigorous model for mass transfer. They considered several packing-specific parameters, enabling them to capture differences in the performance of similar packings. However, no random packings were used in the study. Furthermore, many of the packing-specific parameters, such as F_{SE}, S, and α, apply only to corrugated sheet structured packing with no analog in other packing types. This makes it impossible to use the correlations with random packings without assuming values for these parameters.

Hanley and Chen developed mass transfer correlations for use in the Aspen Plus process simulator [Hanley and Chen, 2012]. The correlations use empirical relationships for both mass transfer coefficients and effective interfacial area. Separate correlations were regressed for different pack-

ing types. The correlations are given in Equations 2.20-2.22.

$$Sh_G = \begin{cases} 0.00104 Re_G Sc_G^{1/3} & \text{for Metal Pall Rings} \\ 0.00473 Re_G Sc_G^{1/3} & \text{for Metal IMTP} \\ 0.0084 Re_G Sc_G^{1/3} \left(\frac{\cos\alpha}{\cos\pi/4}\right)^{-7.15} & \text{for Metal Structured Packing} \end{cases} \tag{2.20}$$

$$Sh_L = \begin{cases} Re_L Sc_L^{1/3} & \text{for Metal Pall Rings and IMTP} \\ 0.33 Re_L Sc_L^{1/3} & \text{for Metal Structured Packing} \end{cases} \tag{2.21}$$

$$\frac{a_e}{a_p} = \begin{cases} 0.25 Re_G^{0.134} Re_L^{0.205} We_L^{0.075} Fr_L^{-0.164} \left(\frac{\rho_G}{\rho_L}\right)^{-0.154} \left(\frac{\mu_G}{\mu_L}\right)^{0.195} & \text{for Metal Pall Rings} \\ 0.332 Re_G^{0.132} Re_L^{-0.102} We_L^{0.194} Fr_L^{-0.2} \left(\frac{\rho_G}{\rho_L}\right)^{-0.154} \left(\frac{\mu_G}{\mu_L}\right)^{0.195} & \text{for Metal IMTP} \\ 0.539 Re_G^{0.145} Re_L^{-0.153} We_L^{0.2} Fr_L^{-0.2} \left(\frac{\rho_G}{\rho_L}\right)^{-0.033} \left(\frac{\mu_G}{\mu_L}\right)^{0.090} \left(\frac{\cos\alpha}{\cos\pi/4}\right)^{4.078} & \text{for Metal Structured Packing} \end{cases} \tag{2.22}$$

The hydraulic diameter in this context is defined as $d_h = 4\varepsilon/a_p$. Systems with amine solvents were analyzed in their study, making the Hanley and Chen correlations particularly relevant for CO_2 absorption processes. However, the correlations are purely empirical, and their predictive ability for packings, systems, and operating conditions outside of those used in the study is questionable. Even for the packings used in the study, the correlations tend to overestimate the effective interfacial mass transfer area at low liquid superficial velocities.

2.2 Packed Column Data

The Process Science and Technology Center (PSTC) at the University of Texas in Austin operates a staged column that is used to collect absorption data for both random and structured packings. Many of these data have been published in theses and dissertations written by graduate students in the group [Wilson, 2004, Tsai, 2010, Wang, 2015, Song, 2017]. With these theses and dissertations, the PSTC offers an extensive database for validation of mass transfer correlations.

PSTC mass transfer data comes from experiments with CO_2-air/NaOH-water, SO_2-air/NaOH-

water, and air/toluene-water systems in packed columns. CO_2-air/NaOH-water experiments are used to determine a_e, SO_2-air/NaOH-water experiments are used to determine k_G, and air/toluene-water experiments are used to determine k_L. In CO_2-air/NaOH-water experiments, inlet and outlet gas phase CO_2 concentrations and temperatures and the superficial velocities of the gas and liquid phases are measured. With knowledge of these parameters, a_e can be calculated by taking a material balance around the packed column. Assuming CO_2 is dilute in the gas phase and the equilibrium concentration of CO_2 in the gas phase is zero, Equations 1.1-1.2 can be simplified and combined to form Equation 2.23.

$$- u_G dy_{CO_2} = K_{OG} a_e y_{CO_2} dh \tag{2.23}$$

Assuming u_G, K_{OG}, and a_e are constant throughout the column, Equation 2.23 can be integrated across the height of the column to produce Equation 2.24.

$$K_{OG} a_e = \frac{u_G}{Z} \ln \frac{y_{CO_2,in}}{y_{CO_2,out}} \tag{2.24}$$

Like alkanolamines, NaOH promotes CO_2 absorption by facilitating acid-base reactions in the liquid phase. The liquid phase mass transfer coefficient is therefore amplified by an enhancement factor, so Equation 1.7 is applicable for this system. If the CO_2-NaOH reaction is taken to be first order, the enhancement factor has the following definition

$$E = \sqrt{1 + \frac{k_{OH^-}[OH^-] D_{CO_2,L}}{k_L^2}} \tag{2.25}$$

where k_{OH^-} is the reaction rate constant. The CO_2-NaOH reaction is considered to be the rate-limiting step in CO_2 absorption for this system [Wang et al., 2016]. Additionally, the reaction rate is considered to be much greater than the mass transfer rate of CO_2 from the gas-liquid interface to the bulk liquid phase. Under these circumstances, the 1 term under the square root in Equation 2.25 and the $1/k_G$ term in Equation 1.7 can be negated. Assuming the ideal gas law is valid, this

allows for the following approximation

$$\frac{1}{K_{OG}} \approx \frac{1}{\sqrt{k_{OH^-}[OH^-]D_{CO_2,L}}} \frac{H_{CO_2}}{RT} \tag{2.26}$$

Combining Equations 2.24 and 2.26 creates the following expression

$$a_e = \frac{u_G}{ZRT} \frac{H_{CO_2}}{\sqrt{k_{OH^-}[OH^-]D_{CO_2,L}}} \ln \frac{y_{CO_2,in}}{y_{CO_2,out}} \tag{2.27}$$

which can be used to calculate a_e in CO_2-air/NaOH-water systems.

The gas phase mass transfer coefficient in a packed column can be calculated with data from SO_2-air/NaOH-water experiments. Like CO_2 absorption, SO_2 absorption is enhanced by liquid phase reactions with NaOH. However, NaOH reacts more aggressively with SO_2 than CO_2. Because of this, SO_2 absorption is considered to be limited by gas phase mass transfer rather than the reaction with NaOH. This allows for an alternative approximation of Equation 1.7 in which the liquid phase mass transfer term rather than the gas phase mass transfer term can be negated. For SO_2-air/NaOH-water systems, the following approximation is used

$$\frac{1}{K_{OG}} \approx \frac{1}{k_G} \tag{2.28}$$

which allows for the following analogous form of Equation 2.24.

$$k_G = \frac{u_G}{a_e Z} \ln \frac{y_{SO_2,in}}{y_{SO_2,out}} \tag{2.29}$$

Equation 2.29 is used to calculate k_G in these experiments. u_G, $y_{SO_2,in}$, and $y_{SO_2,out}$ are directly measured. The value of a_e is taken from a CO_2-air/NaOH-water experiment in which the same packing and superficial gas and liquid phase velocities were used.

Data from air/toluene-water experiments are used to calculate the liquid phase mass transfer coefficient. In the air/toluene-water system, toluene is stripped from an aqueous solution by air.

Since the component moving between phases originates in the liquid phase, mass transfer is analyzed from the liquid phase perspective rather than the gas phase perspective. The analogous form of Equation 1.2 for the liquid phase perspective is

$$(-N_A) = K_{OL} c_L (x_A - x_A^*) \tag{2.30}$$

where K_{OL} is the overall liquid phase mass transfer coefficient. An analogous form of Equation 1.5 can be used to calculate K_{OL}. Unlike the CO_2-air/NaOH-water and SO_2-air/NaOH-water systems, the air/toluene-water system involves no chemical reactions. Toluene stripping is assumed to be limited by liquid phase mass transfer, so K_{OL} can be approximated as

$$\frac{1}{K_{OL}} \approx \frac{1}{k_L} \tag{2.31}$$

Using this approximation with a mass balance on liquid phase toluene integrated across the height of the packed column gives Equation 2.32

$$k_L = \frac{u_L}{a_e Z} \ln \frac{x_{toluene,in}}{x_{toluene,out}} \tag{2.32}$$

which can be used to calculate k_L. Similar to the SO_2-air/NaOH-water experiments, u_L, $x_{toluene,in}$, and $x_{toluene,out}$ are directly measured, while a_e is determined from a comparable CO_2-air/NaOH-water experiment.

3. PROBLEM STATEMENT AND APPROACH

3.1 Problem Statement

Carbon capture and storage technologies offer a way to reduce greenhouse gas emissions associated with the US energy industry. Because they can be retrofitted to existing fossil fuel combustion processes, they are a more immediately viable solution than replacement with alternative energy sources. The most feasible process for carbon capture in the present day is CO_2 absorption with MEA in a staged column, and the use of packing instead of trays inside the column can offer several advantages. However, rigorous simulation of a packed absorber column for design and analysis purposes requires mass transfer modeling. This in turn requires knowledge of the gas and liquid phase mass transfer coefficients and effective interfacial mass transfer area.

Despite the existence of many correlations for mass transfer parameters in literature, no single set of correlation is accurate across the entire range of gas/liquid systems, column operating conditions, and packing types. Furthermore, the continuous development of new types of random and structured packings inevitably creates scenarios for which a particular mass transfer correlation is not applicable. For these reasons, additional development and validation of mass transfer correlations with experimental data for random and structured packings is needed.

The objective of this thesis is to develop a set mass transfer correlations and use them in modeling a carbon capture CO_2 absorption unit. Correlations will be developed for the gas and liquid phase mass transfer coefficients and the effective interfacial mass transfer area. The correlations will consider both extensive and intensive properties of the gas and liquid in the column, such as superficial velocities, densities, viscosities, and surface tension. They will also consider parameters specific to the type of packing used and have relevance for both random and structured packings. Data sets published by the Process Science and Technology Center at the University of Texas in Austin will be used to validate the correlations and compare their accuracy to that of other literature correlations. Using the newly developed correlations in conjunction with the process simulation

software ProMax, a design and economic analysis of a CO_2 absorber column will be performed.

3.2 Approach

A diagram of the workflow for this thesis is given in Figure 3.1. The work of this thesis can be divided into four main sequential parts.

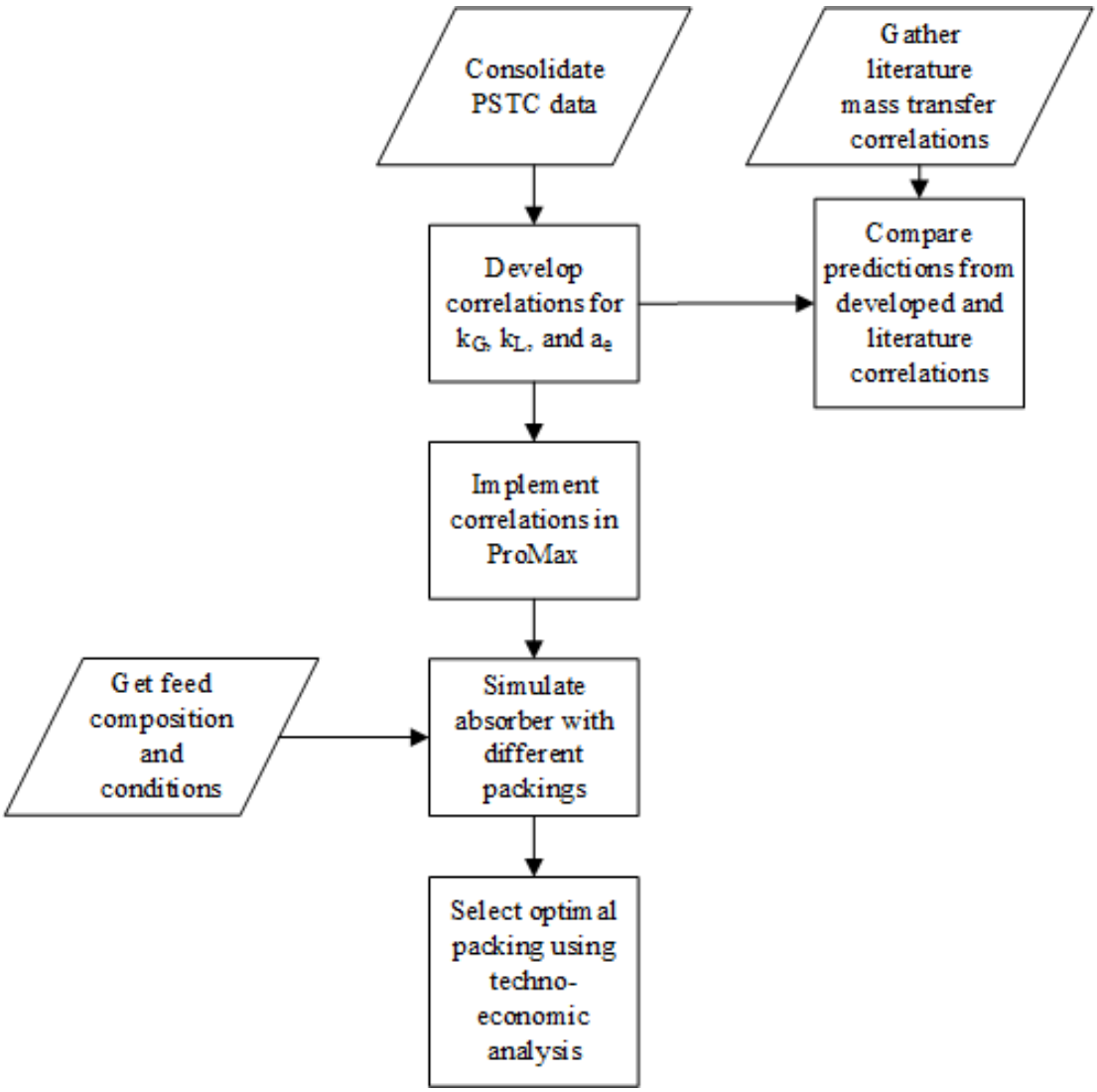

Figure 3.1: Thesis workflow diagram.

First, published mass transfer data from the PSTC will be used to develop mass transfer correlations for the gas phase mass transfer coefficient, liquid phase mass transfer coefficient, and

effective interfacial mass transfer area. This involves consolidating data from several published theses and dissertations from the PSTC group. The data will be analyzed to observe trends with respect to gas and liquid phase physical properties, superficial velocities, and packing parameters. Expressions for the three mass transfer parameters will then be regressed to fit these trends.

Second, predictions from the developed correlations will be compared against those of several literature correlations and experimentally determined values in the PSTC database. Differences between the predicted and experimental values of the three mass transfer parameters will be used to assess the relative accuracy of each correlation.

Third, the developed correlations will be incorporated into ProMax. The correlations will be made available as a "User Defined" mass transfer correlation in the software's distillation column block.

Finally, an absorber for a carbon capture CO_2 absorption unit will be designed using the developed correlations, and an economic analysis of the column will be performed. A model for an absorber with a feed stream representative of flue gas from a power plant will be simulated in ProMax. The column height and diameter required to meet a CO_2 specification in the treated flue gas will be determined for several random and structured packings. The capital and utility costs incurred by each packing will be estimated, and the packing that offers the lowest cost will be identified as the optimal packing for use in the absorber.

4. METHODOLOGY

4.1 Mass Transfer Correlation Development

Mass transfer data taken in a pilot-scale packed absorber and published by the PSTC group at the University of Texas in Austin was consolidated. The data was sourced from one Master of Science thesis and three PhD dissertations [Wilson, 2004, Tsai, 2010, Wang, 2015, Song, 2017]. A summary of the data sources used in this work is given in Table 4.1. The data consists of measured

Source	# of a_e Data Points	# of k_G Data Points	# of k_L Data Points
Wilson (2004)	178	0	0
Tsai (2010)	457	0	0
Wang (2015)	208	51	75
Song (2017)	107	14	240

Table 4.1: Sources of mass transfer data.

a_e, k_G, and k_L values with corresponding operating conditions and physical properties of the gas-liquid system. As discussed in Chapter 2, a_e values were determined using a CO_2-air/NaOH-water system, k_G values were determined using an SO_2-air/NaOH-water system, and k_L values were determined using an air/toluene-water system. For some experiments, the aqueous liquid phase was modified with additives to change viscosity or surface tension. These additives were non-reactive and included glycol and proprietary surfactant and polymer solutions [Tsai, 2010, Song, 2017].

A total of 27 different packings were represented in the PSTC data. 10 of these were random packings, and the remaining 17 were corrugated sheet structured packings. Properties and number of associated data points of the random packings and structured packings are given in Tables 4.2 and 4.3, respectively. All packing property values shown were taken from the PSTC data sources, except those marked with an "*". These were estimated based on values reported for similar packings.

Packing Name	a_p (m^2/m^3)	d_p (m)	ε	# of $a_e/k_G/k_L$ Data Points
1" Pall Rings	184	0.025	0.96	21
2" Pall Rings	115	0.051	0.98	16
IMTP 25	230	0.025	0.97	24
IMTP 40	165	0.04	0.98	24
CMR-2	148	0.051	0.97	24
CMR-2A (Plastic)	106	0.051	0.97	24
RSR 0.3	315	0.015	0.96	17/4/10
RSR 0.5	250	0.02	0.97	18
RSR 0.7	180	0.025	0.98	23/6/7
RSR 1.5	120	0.045*	0.98	23/5/30

Table 4.2: Random packing properties and number of available data points. *Values estimated based on similar packings.

Packing Name	a_p (m^2/m^3)	ε	α (°)	S (m)	B (m)	h (m)	# of $a_e/k_G/k_L$ Data Points
Flexipac 1Y	410	0.91	45	0.009	0.0127	0.0064	26
GT-OPTIM PAK 250Y	250	0.95*	45	0.016	0.027	0.01	62/4/75
GT-PAK 350Y	350	0.95	45	0.013	0.0167	0.00754	19/7/38
GT-PAK 350Z	350	0.95	70	0.011	0.0175	0.00794	25/5/8
GT-PAK 500Y	500	0.95	45	0.008	0.0143	0.00635	14/6/9
Mellapak 125Y	125	0.99	45	0.037	0.055	0.0248	66/5/29
Mellapak 250X	250	0.98	60	0.017	0.0241	0.0119	89/6/34
Mellapak 250Y	250	0.95	45	0.017	0.0241	0.0119	121/6/34
Mellapak 250Y (smooth)	250	0.95	45	0.017	0.0241	0.0119	44
Mellapak 2X	205	0.99	60	0.019	0.0318	0.0.0143	27/6/9
Mellapak 2Y	205	0.99	45	0.0215	0.033	0.0138	21
Mellapak 500Y	500	0.92	45	0.0081	0.0096	0.00653	92
MellapakPlus 252Y	250	0.98	45	0.017	0.0241	0.0119	63
Montz B1-250	250	0.98	45	0.017	0.023	0.012	24
Montz B1-250MN	250	0.98*	45	0.016	0.022	0.011	22/5/32
Montz B1-500 (Plastic)	500	0.93	45	0.0081*	0.0096*	0.00653*	21

Table 4.3: Structured packing properties and number of available data points. *Values estimated based on similar packings.

Overall, the packing specific areas ranged from 106 to 500m^2/m^3. The random packings were modern random packings with complex geometries. Four different types were included: Pall rings, Intalox Metal Tower Packing (IMTP), Cascade Mini-Rings (CMR), and Raschig Super-Rings (RSR). For each type, multiple sizes were tested. Similarly, the structured packings consisted of sets from four types: Flexipac, GT-PAK (including GT-OPTIM PAK), Mellapak (including MellapakPlus), and Montz. Various corrugation angles and corrugation dimensions were represented. One plastic random packing and one plastic structured packing (CMR-2A and Montz B1-500, respectively) were used, with the remaining packings being metal.

The physical properties varied in the PSTC a_e experiments were u_L, u_G, μ_L, ρ_L, and σ. ρ_L was not varied directly; differences in ρ_L throughout the database were attributable to minute changes in column temperature and introduction of non-reactive liquid additives meant to change σ or μ_L. Therefore, trends in a_e with respect to u_L, u_G, μ_L, and σ were analyzed as a starting point for developing a correlation to fit the data. The properties that were believed to have a significant effect on a_e were organized into dimensionless groups, and an expression for the dimensionless effective interfacial mass transfer area, a_e/a_p, in terms of these groups was regressed. The expression was assumed to be of the power law form, where a_e/a_p is the product of the dimensionless groups and a constant with each group raised to a certain power. Most literature correlations developed for effective interfacial mass transfer area, including the ones analyzed in this work, are power law relationships in terms of dimensionless groups [Hanley and Chen, 2012].

Regression of a correlation for a_e consisted of determining values for the exponents of the dimensionless groups and the constant in the power law relationship. To simplify the regression, the natural logarithm of both sides of the equation were taken. This made the equation linear with respect to the power law exponents and the natural logarithm of the constant. The Solver add-in in Microsoft Excel was used to determine the exponent and constant values that minimized the sum of the squared $\ln a_e/a_p$ residuals. Since the sum of the squared residuals as a function of the exponents and natural logarithm of the constant was smooth and quadratic, "GRG Nonlinear" was used as the algorithm in the solver.

The methodology for developing correlations for k_G and k_L was similar to that of a_e. In the PSTC k_G experiments, u_L and u_G were varied. In the k_L experiments, u_L, u_G, and μ_L were varied. Changing values of ρ_L and D_L are also found in the database, but as was the case with ρ_L in the a_e experiments, these variations were a by-product of variations in μ_L rather than experimental design.

4.2 Mass Transfer Correlation Comparison

Predictions from five sets of literature mass transfer correlations were compared against experimental values from the PSTC data and predictions from the mass transfer correlations developed in this work. The Onda; Bravo and Fair; Billet and Schultes; Rocha, Bravo, and Fair; and Hanley and Chen correlations were used. Each of these literature correlations is described in Chapter 2. To avoid correlation misuse, each correlation was only tested with data for packings to which the correlation is considered applicable. The Onda and Bravo and Fair correlations were tested with all random packing data points. The Rocha, Bravo, and Fair correlations were tested with all structured packing data points. The Hanley and Chen correlations were tested with data points for Pall rings, IMTP, and metal structured packing. Only the Billet and Schultes correlations were tested with all data points in the PSTC database.

Some of the literature correlations utilize material or packing-specific constants. The Onda correlation for a_e requires a critical surface tension (σ_c) that depends on packing material of construction. Values in Table 2.4 for metal and plastic were used in evaluating the Onda correlation for random packings. The Rocha, Bravo, and Fair correlations use a surface enhancement factor (F_{SE}) to account for the effect of structured packing surface texture on mass transfer. All metal structured packings analyzed in this work are assumed to have an F_{SE} of 0.35, and all plastic structured packings are assumed to have an F_{SE} of 0.46. These values are based on reported F_{SE} values for metal Flexipac and plastic Mellapak packings [Rocha et al., 1993]. Finally, the Billet and Schultes correlations for mass transfer coefficients utilize dimensionless packing-specific constants (C_G and C_L). Relevant values for these constants are given in Table 4.4. Values marked with "*" were taken from defaults found in ProMax, those marked with "**" are estimated based on values for similar

packings, and all others were taken from literature [Billet and Schultes, 1999].

Packing Name	C_G	C_L
1" Pall Rings	0.336	1.44
2" Pall Rings	0.410	1.192
IMTP 25	0.52*	1.45*
IMTP 40	0.4*	1.3*
CMR-2	0.4*	1.3*
CMR-2A (Plastic)	0.37*	1.5*
RSR 0.3	0.45	1.5
RSR 0.5	0.43	1.45
RSR 0.7	0.43**	1.45**
RSR 1.5	0.43**	1.45**
Flexipac 1Y	0.515**	1.354**
GT-OPTIM PAK 250Y	0.377**	0.992**
GT-PAK 350Y	0.377**	0.992**
GT-PAK 350Z	0.377**	0.992**
GT-PAK 500Y	0.515**	1.354**
Mellapak 125Y	0.215*	0.565*
Mellapak 250X	0.302*	0.794*
Mellapak 250Y	0.377*	0.992*
Mellapak 250Y (smooth)	0.377**	0.992**
Mellapak 2X	0.237*	0.622*
Mellapak 2Y	0.363*	0954*
Mellapak 500Y	0.515*	1.354*
MellapakPlus 252Y	0.377*	0.992*
Montz B1-250	0.377**	0.992**
Montz B1-250MN	0.377**	0.992**
Montz B1-500 (Plastic)	0.515*	1.354*

Table 4.4: Values of packing-specific constants used in Billet and Schultes correlations.

4.3 ProMax Model Development

The mass transfer correlations developed in this work were incorporated into the process simulator ProMax for use in the software's distillation column block. The ProMax software version used in this work is 5.0.20259. By default, ProMax only supports the Onda; Bravo and Fair; Billet and Schultes; Rocha, Bravo, and Fair; and Hanley and Chen correlations discussed above. How-

ever, it offers the ability for users to import their own custom set of mass transfer correlations. Users can then specify for any stage or stages in a distillation column blog to use the custom correlations instead of one of the aforementioned default correlations to calculate mass transfer coefficients and effective interfacial area.

A detailed description of how to create and use custom mass transfer correlations is found in the help files included with the ProMax software [BRE, 2020b]. The help page titled "User Defined Mass Transfer Coefficient Information" and the "Mass Transfer" section of the "About Advanced Examples" are particularly relevant. Generally, the process involves writing code to implement the desired custom correlations, compiling the code into a *.dll assembly, specifying the location of the assembly in a ProMax distillation column block, and selecting the "User Defined" option for either "Random Mass Transfer Correlation" or "Structured Mass Transfer Correlation". An example code project containing implementations of a custom set of correlations (in this case the Onda correlations) is available in the ProMax example files. The code project can be found by opening ProMax, selecting "Open Example (as read-only)" in the "Create a new project using" section of the "ProMax Project Selection" dialog, and navigating to ..\Advanced Examples\Mass Transfer\UserDefinedMassTransferCoefficients. This code project was used as a starting point for importing the mass transfer correlations developed in this work into ProMax.

Microsoft Visual Studio was used to open the "UserDefinedMassTransferCoefficients.sln" solution file in the above file path and subsequently view, edit, and compile the example code project. The Visual Studio solution contains two projects: "CPPCOM_RandomPacking_UDMTC" and "CSCLR_RandomPacking_UDMTC". Each project contains an implementation of the Onda mass transfer correlations able to be imported into ProMax. "CPPCOM_RandomPacking_UDMTC" is written in C++, and "CSCLR_RandomPacking_UDMTC" is written in C#. Only the project written in C# was utilized as a basis for implementing the developed mass transfer correlations. Either project could have been utilized, but the project written in C# was chosen because of the simpler syntax, smaller amount of required boilerplate code, and author's familiarity with C# compared to C++.

The "CSCLR_RandomPacking_UDMTC" project contains only one file of relevant C# code, which is named "CSCLR_UserDefinedMTC.cs". The file contains a class of the same name that inherits from two ProMax interfaces: "Extensibility.UserDefinedMassTransfer" and "Extensibility.PersistStreamInit". Methods on these interfaces are called by the ProMax source code to perform tasks related to calculating mass transfer parameters and managing resources used in the calculations. Only three of these methods were actually implemented in the original example code and later modified to accommodate the code for the developed mass transfer correlation. "InitNew" is used to create the ProMax properties displayed in the "User Defined Coefficients" tab of the distillation column block window. "InitBeforeCalculate" is called before ProMax solves a column block and is used to cache values of properties that do not change throughout the column profile. Finally, "Individual_K" is called whenever ProMax solves a stage in the column and is used to calculate the gas and liquid phase mass transfer coefficients and effective interfacial mass transfer area. Once calculated, the values for the gas and liquid phase coefficients and interfacial area are assigned to the method's "KV", "KL", and "Area" arguments, respectively. Since the distillation column block can handle multicomponent distillation, "KV" and "KL" consist of 2-D N x N arrays containing binary component mass transfer coefficients, where N is the number of components in the ProMax environment.

The "InitNew", "InitBeforeCalculated", and "Individual_K" methods in the "CSCLR_ UserDefinedMTC" class were modified to replace the Onda mass transfer correlations with the mass transfer correlations developed in this work. The resulting code is given in Appendix A. The solution containing the code was compiled using the "Release" configuration in Visual Studio, and the produced *.dll assembly was used as the source of the "User Defined" mass transfer correlation in the ProMax distillation column block. Details about how the "User Defined" mass transfer correlation was setup and utilized to simulate a packed CO_2 absorber are given in the next section.

4.4 Design and Economic Analysis

A CO_2 absorber suitable for post-combustion CO_2 capture was designed and analyzed. The absorber column was simulated in isolation. Conditions for the flue gas feed to the bottom of

the absorber and lean solvent feed to the top were specified. Assumptions were made about the performance of the stripper column to determine the lean solvent composition. Several random and structured packings were tested in the absorber, and the required column diameter and height associated with each packing were calculated. These values were used to select an optimal packing type and size.

ProMax was used to simulate the CO_2 absorber for design and analysis. The "Amine Sweetening-PR" property package was used in the environment. This property package uses the Peng-Robinson equation-of-state to calculate thermodynamic properties of the gas phase and an electrolytic excess Gibbs free energy model to calculate thermodynamic properties of the liquid phase. Since the liquid phase reaction of CO_2 with alkanolamines forms ions, this property package is well-suited for simulating CO_2 absorption processes.

The conditions of the gas feed to the absorber column were selected to be representative of a flue gas stream from a coal-fired power plant. Table 4.5 shows the feed stream specifications [Aboudheir and McIntyre, 2009]. The flow rate roughly corresponds to the flue gas output of a 50

Property	Value	Units
Temperature	82.2	°C
Pressure	101.325	kPa
Standard Vapor Volumetric Flow	70.8	Nm^3/s
N_2	63.47	mol%
CO_2	12	mol%
H_2O	18.5	mol%
O_2	6	mol%
SO_2	120	ppm
NO	179	ppm
NO_2	7	ppm

Table 4.5: Inlet flue gas specifications.

MW plant [Tsai, 2010]. The pressure is near atmospheric. In addition to CO_2, the feed contains small but significant amounts of SO_2, NO, and NO_2, which are also environmental pollutants

readily absorbed by alkanolamine solutions. In some absorption units, a separate absorber column or column section is used upstream of the absorber for the selective removal of these gases. SO_2 in particular is often targeted for removal because it can react with alkanolamines to form heat-stable salts [BRE, 2020a]. Consistent formation of heat-stable salts reduces the concentration of alkanolamine in the liquid solvent available for CO_2 absorption over time, necessitating additional process measures to regenerate the solvent. Although avoidance of heat-stable salts is important to the performance of a CO_2 absorption unit, the design and analysis of an SO_2 removal system is omitted from this work for the sake of simplicity.

The ProMax flowsheet used for simulation of the isolated absorber column is shown in Figure 4.1. The flue gas inlet passes through a blower before entering the absorber column. Since the

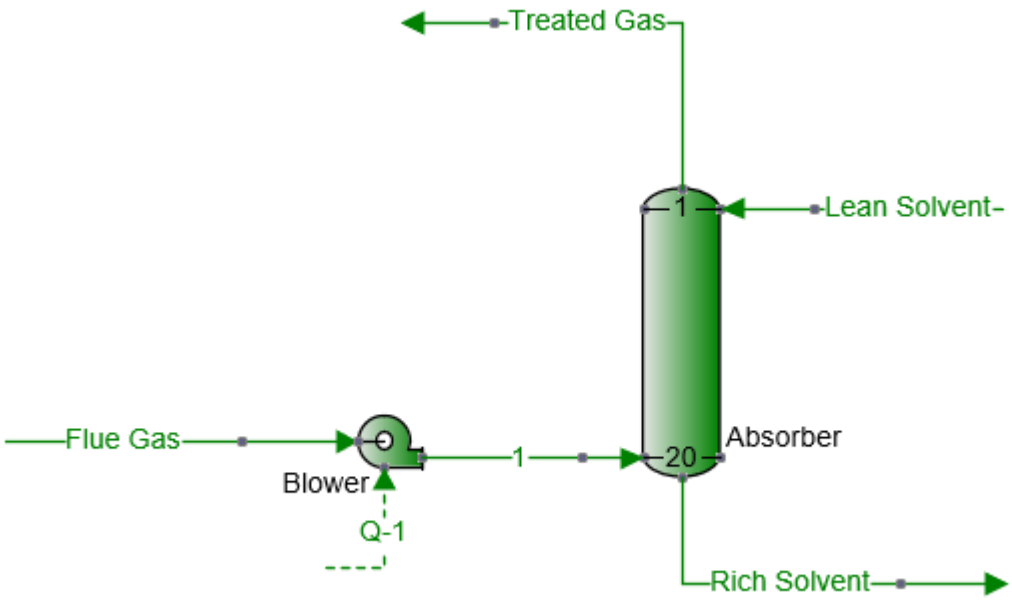

Figure 4.1: ProMax absorber flowsheet.

flue gas is at atmospheric pressure, the blower is required to increase the pressure of the flue gas enough to compensate for the pressure drop in the absorber. The polytropic efficiency of the blower was assumed to be 75%. The top-stage pressure of the absorber was specified as 101.325 kPa. 30

wt% MEA in water was used as the solvent in the absorption unit. A lean loading of 0.10 mol CO_2/mol MEA, or about 2.17 wt% CO_2 in the lean solvent stream, was assumed in the absence of a simulated regenerator. The flow rate of the solvent was adjusted to make the rich loading 0.35 mol CO_2/mol MEA. This was done automatically using a ProMax simple solver set on the standard liquid volumetric flow rate of the lean solvent. Rich loading was calculated using an amine analysis on the rich solvent stream and imported into the simple solver as a measured variable. The values selected for MEA concentration and rich loading correspond to the upper-limit values generally imposed to limit solvent corrosivity, as discussed in Chapter 1.

The absorber column was modeled using the "Mass + Heat Transfer (Reactive & Non-Reactive)" model type. "TSWEET Absorber/Stripper" was used for the "Mass + Heat Transfer Column Type" to account for the kinetics of the liquid phase reactions in the column. The "Mass Transfer Formulation" was set to "General Maxwell-Stefan". In the "Stages" tab of the column Project Viewer window, the "Pressures from Hardware" option was selected. This allowed for the pressure profile in the column to be calculated rather than user specified. In the "Convergence" tab of the column Project Viewer window, the "Enthalpy Model" was set to "Composition-Dependent". Selecting this option seemed to improve the likelihood of column convergence. In the "Mass Transfer" tab, both the "Random Mass Transfer Correlation" and the "Structured Mass Transfer Correlation" were set to "User Defined" for all stages. In the "User Defined Coefficients" tab, the "Extensibility Package Type" was changed to "CLR", and the file path to the compiled *.dll assembly discussed in Section 4.3 was specified in the "CLR Assembly Name or Path" box. The "CLR Implementation Class" was specified as "CSCLR_RandomPacking_UDMTC.CSCLR_UserDefinedMTC", which corresponds to the namespace and class containing the custom mass transfer correlation code. With these specifications in place, the distillation column block simulating the absorber was set up to use the mass transfer correlations developed in this work instead of the default correlations in ProMax.

Three random and four structured packings were selected for testing in the isolated absorber column flowsheet. The random packings were Raschig Super-Rings of size 0.3, 0.7, and 1.5. The structured packings were Mellapak 125Y, Mellapak 250X, Mellapak 250Y, and GT-PAK 500Y.

These seven packings were chosen because they collectively covered much of the range of the PSTC database in terms of packing properties. The specific areas range from 120 to 500 m^2/m^3, void fractions range from 0.95 to 0.99, and structured packing corrugation angles include both 45°and 60°. Additionally, the data for these packings included values for all three mass transfer parameters (a_e, k_G, and k_L). Using all three of the developed mass transfer correlations in the context of simulating a CO_2 absorber column is therefore less of an extrapolation when considering these packings than it would be when considering packings for which there was no data available to fit one of the correlations.

Four of the above seven packings were already available as column hardware options in the ProMax distillation column block. Raschig Super-Rings of sizes 0.7 and 1.5 and GT-PAK 500Y had to be implemented as user-defined packings to be used in ProMax. This was done by modifying the "Column Hardware.xml" file. Instructions for doing this were found in the ProMax help files on the page titled "Column Hardware.xml File" [BRE, 2020b]. Entries for the two random packings and structured packing were added to the *.xml file. The added *.xml code is shown in Appendix B. For the new packings added, values of several constants used in the Billet and Schultes mass transfer and pressure drop correlations were required. The values associated with the new Raschig Super-Ring sizes were linearly interpolated based on those associated with the sizes of metal Raschig Super-Rings already available in ProMax (0.3, 0.5, 1, 2, and 3). The values associated with GT-PAK 500Y were assumed to be the same as those associated with Mellapak 500Y.

Each of the seven packings mentioned above was used in turn to populate all of the absorber column stage internals, the flowsheet was solved, and a suitable column diameter and height were determined. For every packing test, 20 column stages were used. The number of stages in a packed mass and heat transfer model column represents only the number of discrete cross-sectional elements used in solving the column profile, so the choice is somewhat arbitrary. The recommendation is to use one stage per roughly 0.5 m packing, but mass and heat transfer columns with more than about 25 stages can be difficult to converge [BRE, 2020a]. Therefore, 20 served as a good moder-

ate number of stages to use. The system factor for each stage was set to 0.8 to account for foaming tendencies in systems with alkanolamines.

ProMax allows for the specification of either the diameter or the fraction flooding of each stage, with the unspecified property being calculated using the specified property. A fraction flooding of 70% was therefore set for each stage rather than an assumed column diameter. This enabled the calculation of diameters large enough to safeguard against flooding for each tested packing. The total column diameter was taken as the maximum stage diameter calculated. To calculate an appropriate column height, a simple solver was created on the "Total Height" property. The molar flow rates of CO_2 in the flue gas and treated flue gas were added as measured variables, and the simple solver was configured to automatically adjust the column height to reduce the treated gas CO_2 molar flow rate to one tenth of the flue gas CO_2 molar flow rate. The resulting height represented the total height of packing required for 90% CO_2 removal from the flue gas given the above calculated column diameter.

With the absorber column diameter and height required for each tested packing, a cost estimate of the absorber could be performed. The total purchase cost of the column was taken to be a sum of the costs given in Table 4.6 [Seider et al., 2008]. W is the weight of the column shell, which

Cost Component	Expression ($)
Shell	$F_M \exp\left[7.2756 + 0.18255 \ln W(\text{lb}) + 0.02297 \left(\ln W(\text{lb})\right)^2\right]$
Platforms and Ladders	$300.9 d_c(\text{ft})^{0.63316} Z(\text{ft})^{0.80161}$
Packing	$C_{PK} V_{PK}$
Liquid Distributors	$125\pi \left(d_c(\text{ft})/2\right)^2$

Table 4.6: Components of absorber purchase cost.

was calculated using the following equations

$$W = \pi \left(d_c + t_s\right) \left(Z + 0.8 d_c\right) t_s \rho_M \tag{4.1}$$

$$t_s(\text{in}) = \frac{P_d(\text{psig}) d_c(\text{ft})}{1.7 P_{stress}(\text{psig}) - 1.2 P_d(\text{psig})} \tag{4.2}$$

where t_s is the shell thickness, ρ_M is the density of the shell's material of construction, P_d is the design pressure, and P_{stress} is the maximum allowable stress. Since the maximum pressure inside the column is the atmospheric pressure plus the pressure drop incurred by the column, the column operating pressure is expected to be small (< 5 psig). The column operating temperature is governed by the inlet gas and solvent temperatures and the heat of reaction inside the column, but it is expected to be well below 650 °F. Under these conditions, values of 10 and 15000 psig can be assumed for P_d and P_{stress}, respectively. F_M is a cost factor based on the column shell material of construction. Since MEA is corrosive, stainless steel should be used for the interior of the column shell. However, this requirement can be satisfied by having only a thin layer of stainless steel on the interior of the column and letting the bulk of the column shell be constructed of carbon steel. Under this dual-material design, the value of F_M should be somewhere between the values for carbon steel (1.0) and stainless steel (1.7). A value of 1.3 will be used in this work. ρ_M can then be approximated as the density of carbon steel, which is assumed to be 0.284 lb/in^3.

C_{PK} is the cost of the packing per unit volume, and V_{PK} is the volume of packing required. V_{PK} was calculated as the total volume of the packed bed in the absorber column. The following expression was used to estimate C_{PK} for the random packings tested:

$$C_{PK} = 19.02 a_p + 2020 \tag{4.3}$$

This expression was developed based on costs given in Seider et al. for metal Pall rings, which have values of a_p similar to those of Raschig Super-Rings for each nominal packing size. To estimate C_{PK} for the structured packings, Equation 4.4 was used.

$$C_{PK} = 5.37 a_p + 7486 \tag{4.4}$$

The relationship was based on an expression used by Tsai to estimate structured packing costs

[Tsai, 2010]. The expression in its original form predicted costs much lower than those of the random packings, which is the opposite of the expected trend. Therefore, the expression was modified such that the predicted cost of a structured packing with an a_p of 250 m^2/m^3 equaled the rough figure given in Seider et al. for corrugated sheet structured packings (250 $/ft^3). The coefficient for a_p from the original expression was kept, but converted to equivalent $ in Seider et al. using the ratio of the Chemical Engineering Plant Cost Index (CEPCI) in Seider et al. (500) vs the CEPCI from when Tsai developed the original expression (592.2) [CEPCI, 2009].

The choice of packing in the absorber affects the pressure drop through the column in addition to the column dimensions. Since the flue gas blower is designed to compensate for this pressure drop, the choice of packing also indirectly affects the operating conditions and, in turn, the costs associated with the blower. The purchase cost of the blower can be estimated with Equation 4.5.

$$C_{blower} = F_M \exp\left(6.8929 + 0.7900 \ln P_B\right) \tag{4.5}$$

The blower is assumed to have stainless steel blades to protect against corrosion from the acid gases in the inlet flue gas. The corresponding F_M value is 2.5. P_B is the power required by the blower, which is calculated by ProMax. In addition to capital costs, the blower incurs a utility cost in the form of electrical power to the blower motor. The cost of electricity was assumed to be $0.060/kWh [Seider et al., 2008].

The purchase cost of the absorber column, purchase cost of the blower, and utility cost of electricity supplied to the blower were used to compare the various random and structured packings tested. To combine the purchase and utility costs into one metric, a simple 5-year annualized cost was calculated:

$$C_A = C_{elec} + 0.20\left(C_{absorber} + C_{blower}\right) \tag{4.6}$$

C_A was converted to approximate current $ using the ratio of the CEPCI as of May 2020 (593.5) to that used in Seider et al. (500) [CEPCI, 2020]. The packing that allowed for the minimum value of this simple annualized cost was considered the optimal choice for use in the CO_2 absorption unit.

5. RESULTS AND DISCUSSION

5.1 Mass Transfer Correlation Development

5.1.1 Effective Interfacial Mass Transfer Area

Trends in the PSTC database were analyzed to determine which physical and packing properties should be included in the correlation developed for effective interfacial mass transfer area. Figure 5.1 shows data points for the effective interfacial mass transfer area of Mellapak 250Y plotted against the liquid superficial velocity for several superficial gas velocities. All physical properties of the gas and liquid phases are held constant. The liquid superficial velocity clearly

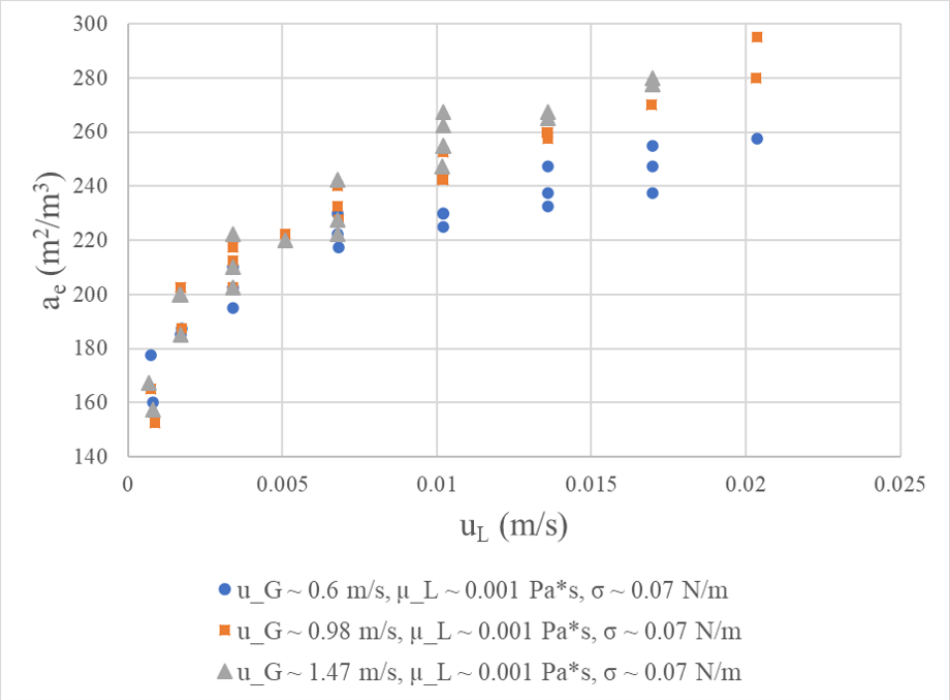

Figure 5.1: Mellapak 250Y effective interfacial mass transfer area vs liquid superficial velocity for different gas superficial velocities.

influences a_e. Although the trend is slight, a_e appears to increase with u_G as well. In Figure 5.2, a_e is once again plotted against u_L, but with a single value for u_G and multiple liquid viscosities.

a_e does not show a clear trend with respect to μ_L. However, a_e appears to increase with surface

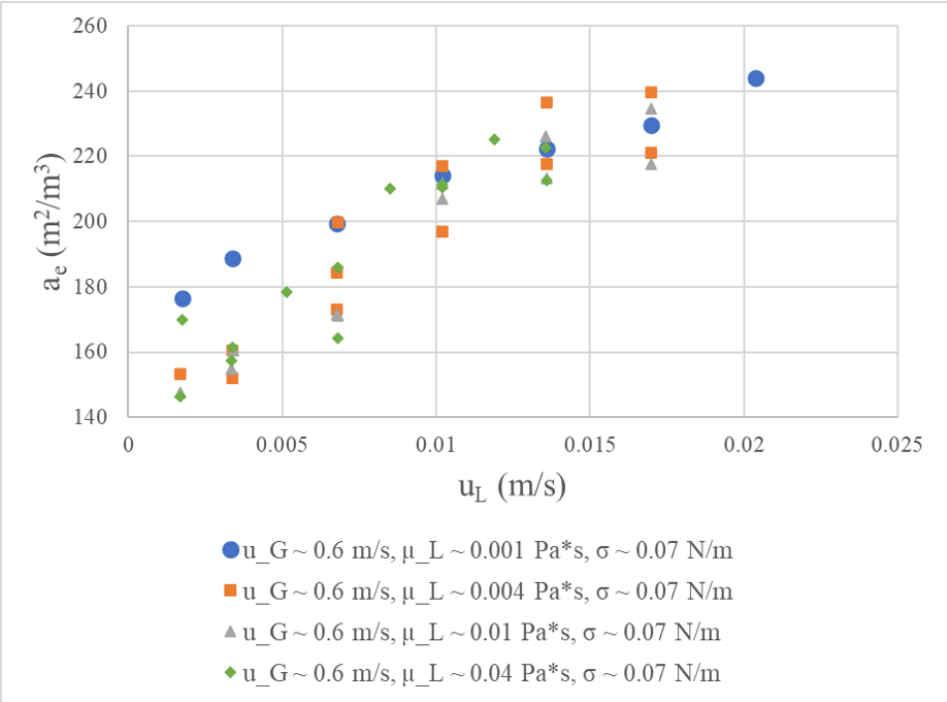

Figure 5.2: GT-OPTIM PAK 250Y effective interfacial mass transfer area vs liquid superficial velocity for different liquid viscosities.

tension, as shown in Figure 5.3. In terms of packing parameters, a_e appears to increase with the corrugation angle in structured packing. As shown in Figure 5.4, GT-PAK 350Z, which has a corrugation angle of 70°, has a consistently higher effective interfacial mass transfer area than that of GT-PAK 350Y (α = 45) when all other physical and packing properties are held constant.

Based on the observed trends above, a_e was taken to be a function of u_G, u_L, and σ. When applied to structured packing, a_e was also taken to be a function of α. To make the correlation for a_e dimensionless, the groups Re_G, Re_L, We_L, Fr_L, and $\frac{\cos\alpha}{\cos\pi/4}$ were chosen for regression. Additionally, a constant, C_M, with different values for metal packings and plastic packings was included to account for the effect of packing material of construction. The definitions for the dimensionless parameters can be found in Chapter 1. Fr_L was included on the semi-theoretical

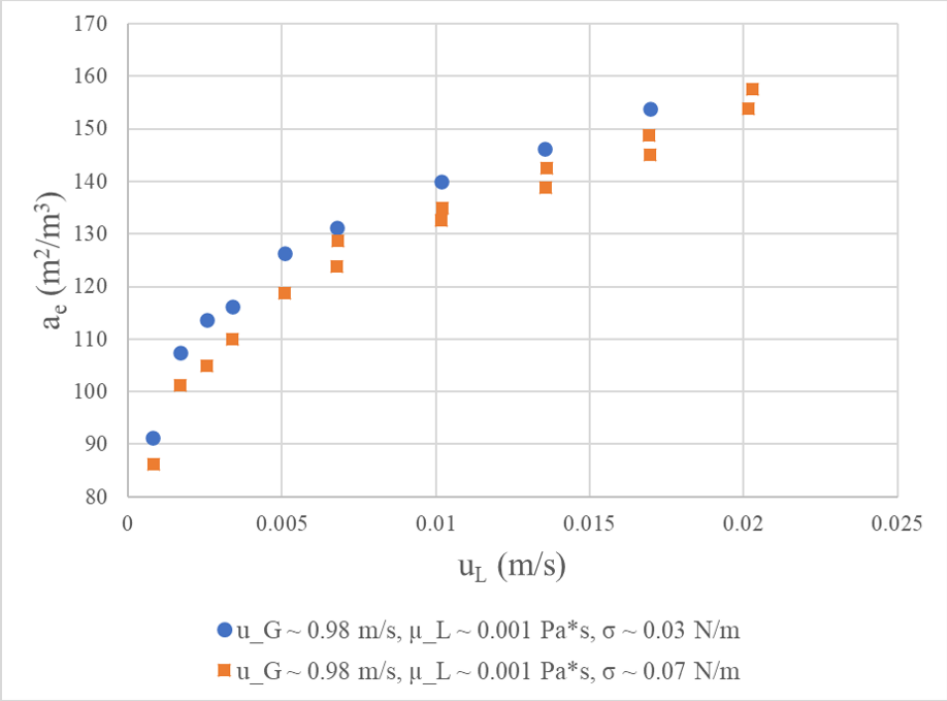

Figure 5.3: Mellapak 125Y effective interfacial mass transfer area vs liquid superficial velocity for different surface tensions.

basis that a_e should depend on g due to the fact that liquid flow in a packed column is driven by gravity [Hanley and Chen, 2012]. The denominator $\cos \pi/4$ was chosen in the last term because it reduces the term to 1 when α is 45°. This is the case in all "Y"-type structured packings, which were the largest represented group in the database.

Equation 5.1 was chosen as the form of the a_e correlation. The linearized form used for least-squares regression is given in Equation 5.2.

$$\frac{a_e}{a_p} = C_0 C_M Re_G^{C_1} Re_L^{C_2} We_L^{C_3} Fr_L^{C_4} \left(\frac{\cos \alpha}{\cos \pi/4} \right)^{C_5} \tag{5.1}$$

$$\ln\left(\frac{a_e}{a_p}\right) = \ln C_0 + \ln C_M + C_1 \ln Re_G + C_2 \ln Re_L + C_3 \ln We_L + C_4 \ln Fr_L + C_5 \ln\left(\frac{\cos \alpha}{\cos \pi/4}\right) \tag{5.2}$$

The material factor C_M was given the form $C_M = A^B$, where A is 1 for metal packings and 2 for plastic packings. The least-squares regression problem was then setup to solve for the value

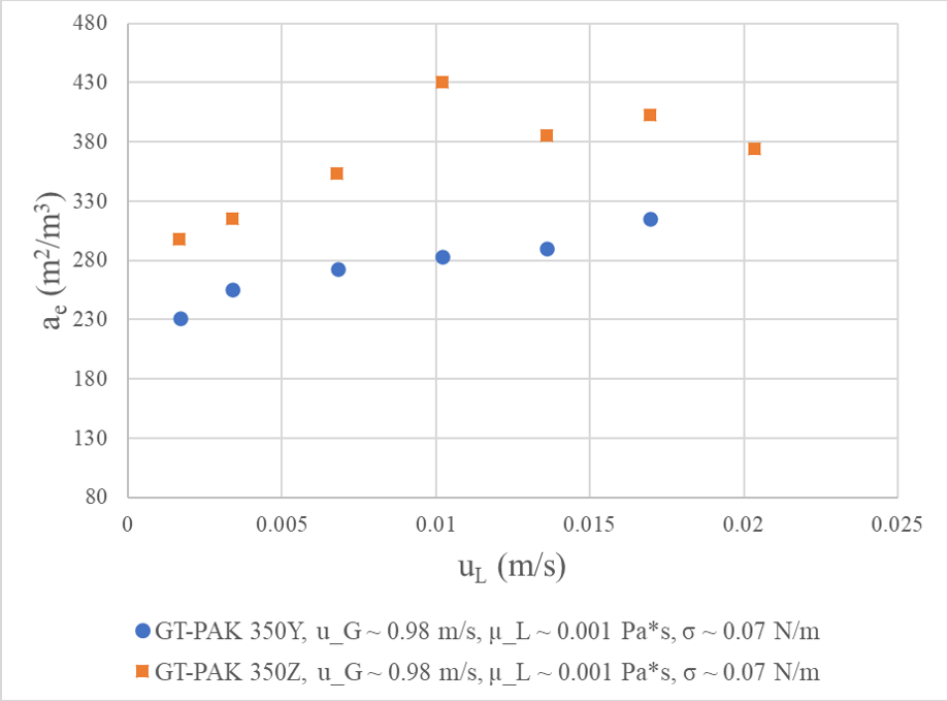

Figure 5.4: Effective interfacial mass transfer area vs liquid superficial velocity for different corrugation angles (GT-PAK 350Y: 45°, GT-PAK 350Z: 70°).

of B rather than C_M directly. Several of the dimensionless groups required a hydraulic diameter (d_h), which is used to represent characteristic packing properties. Regression was performed with several different definitions for d_h taken from literature correlations to determine which gave the best fit. The various forms tested are given in Equation 5.3.

$$d_h = \begin{cases} \frac{1}{a_p}, \frac{4\varepsilon}{a_p} & \text{for random packings} \\ \frac{1}{a_p}, \frac{4\varepsilon}{a_p}, S, \delta_{Nusselt} = \left(\frac{3\mu_L u_L Bh}{4S\rho_L \sin\alpha}\right)^{1/3} & \text{for structured packings} \end{cases} \tag{5.3}$$

$\delta_{Nusselt}$ is a theoretical characteristic length based on the film height of liquid flow down an inclined plane [Tsai, 2010].

The final regressed form of the correlation developed for a_e in this work is given in Equations 5.4-5.6.

$$\frac{a_e}{a_p} = 0.346 C_M Re_G^{0.162} Re_L^{0.0156} We_L^{0.0709} Fr_L^{-0.0104} \left(\frac{\cos\alpha}{\cos\pi/4}\right)^{-0.120} \tag{5.4}$$

$$C_M = \begin{cases} 1.0 & \text{for metal packings} \\ 0.8 & \text{for plastic packings} \end{cases} \tag{5.5}$$

$$d_h = \frac{4\varepsilon}{a_p} \tag{5.6}$$

For random packings, α is assumed to be 45°to make its dimensionless group unity. After regression, the sum of squared residuals across the entire database of 950 a_e values was 15.37. The % error associated with Equation 5.4 calculated for all a_e data points is plotted in Figure 5.5 for random packings and Figure 5.6 for structured packings. Most of the a_e values calculated for random

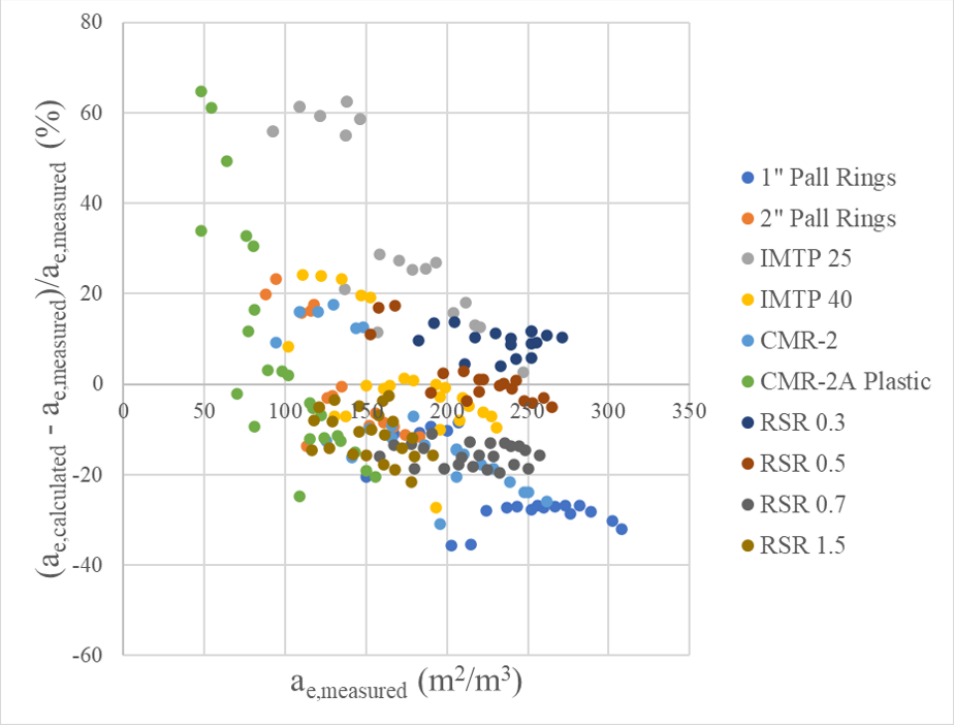

Figure 5.5: % error of a_e calculated by Equation 5.4 for random packings.

packings were within 40% of the corresponding measured a_e values. For structured packings, most were within 30%. The improved accuracy for structured packings was expected due to the fact that structured packings comprised the majority of the database.

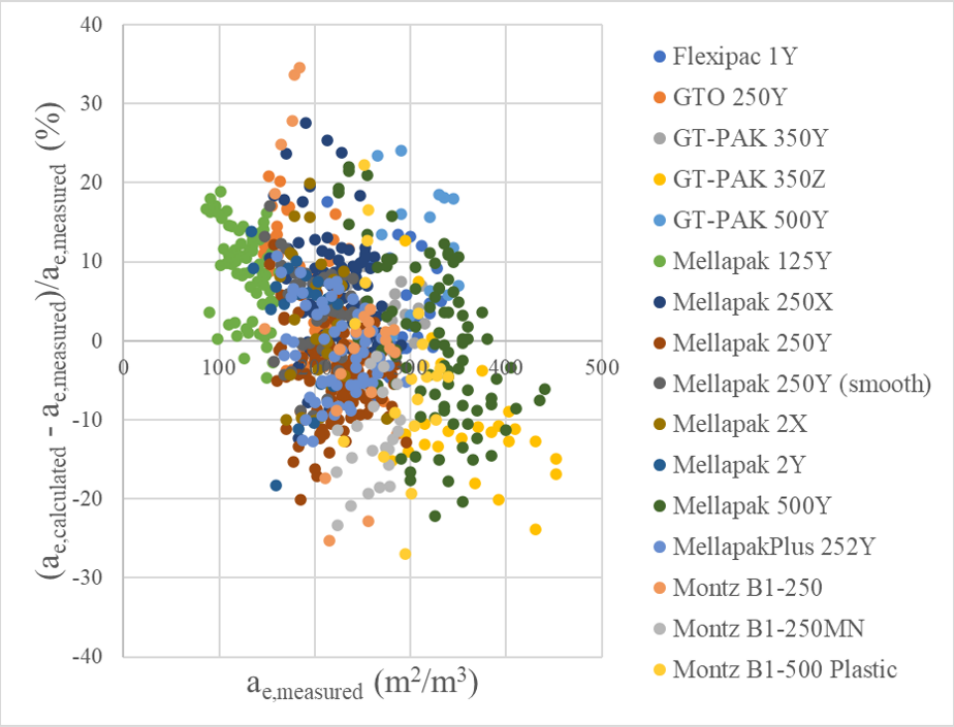

Figure 5.6: % error of a_e calculated by Equation 5.4 for structured packings.

The substituted form of the developed correlation for effective interfacial mass transfer area is given in Equation 5.7.

$$a_e = 0.475 C_M \left(\frac{\rho_G u_G}{\mu_G}\right)^{0.162} \rho_L^{0.0865} u_L^{0.137} \mu_L^{-0.0156} \sigma^{-0.0709} g^{0.0104} \varepsilon^{0.259} a_p^{0.741} (\cos\alpha)^{-0.120} \quad (5.7)$$

Despite the observation that μ_L has no apparent effect on a_e, μ_L had to be included in the correlation in order to make it dimensionless. Likewise, ρ_G, μ_G, and ρ_L were included, even though none of these variables were independently adjusted in the database. The dependency of a_e on each of these parameters in the correlation was a by-product of the dependency of a_e on the dimensionless groups containing the parameter, rather than a dependency on the parameter itself. The dependencies, as determined by the exponents in Equation 5.7, on μ_L and ρ_L were small but non-negligible. However, the dependencies on μ_G and ρ_G were rather significant. To evaluate the sensitivity of the correlation with respect each of these added variables, the regression was re-performed with

a systematic adjustment to each variable independently. The values of μ_L, ρ_L, μ_G, and ρ_G were one-by-one changed by ±10% throughout the entire database, and least-squares regression was once again used to determine the values of the constants in Equation 5.2. This procedure revealed the ranges for each correlation constant expected when any of the above variables differ from their reported database values by up to 10%. The results are shown in Table 5.1 for the constant C_0. For every other constant in the correlation, the range was found to be negligible. The relative

Variable	C_0 with Variable Adjusted by -10%	C_0 with Variable Adjusted by +10%
μ_L	0.346	0.347
ρ_L	0.349	0.343
μ_G	0.340	0.351
ρ_G	0.352	0.341

Table 5.1: Range of C_0 in Equation 5.2 when variable values are systematically adjusted.

effects of the changes to each variable on C_0 corresponded to the relative dependencies of a_e on each variable in Equation 5.7. Changes to μ_G and ρ_G had roughly equal but opposite effects on C_0, with the magnitude of the effects being much greater than those of changes to μ_L and ρ_L. These results indicate the need for further testing of the a_e correlation with data in which μ_G and ρ_G are experimentally varied. Testing the a_e correlation with data taken at different temperatures and pressures, or with a gas phase other than CO_2-air, for instance, would help determine whether the correlation's dependencies on μ_G and ρ_G are valid, or if adjustments to the correlation are needed.

5.1.2 Gas and Liquid Phase Mass Transfer Coefficients

Lack of data for k_G and k_L in which only one physical or packing property differed prevented the type of trend analysis performed for a_e data. Instead, the forms for Sh_G and Sh_L based on commonalities between literature correlations were chosen

$$Sh_G = C_0 Re_G^{C_1} Sc_G^{C_2} \tag{5.8}$$

$$Sh_L = C_0 Re_L^{C_1} Sc_L^{C_2} \tag{5.9}$$

Equations 5.8-5.9 were linearized, and least squares regression was performed to obtain the following correlations for mass transfer coefficients developed in this work.

$$Sh_G = 0.416 Re_G^{0.63} Sc_G^{1/3} \tag{5.10}$$

$$Sh_L = 0.984 Re_L^{0.742} Sc_L^{0.457} \tag{5.11}$$

For Sc_G in Equation 5.10, the Excel Solver converged to a rather large exponent (≥ 3). This appeared to be a case of over-fitting due to lack of data. Instead, an exponent of 1/3 was chosen due to its presence in several literature correlations discussed in Chapter 2.

% error values for Equations 5.10 and 5.11 across the entire database were calculated and plotted in Figures 5.7 and 5.8, respectively. The correlations for k_G and k_L fit their data much

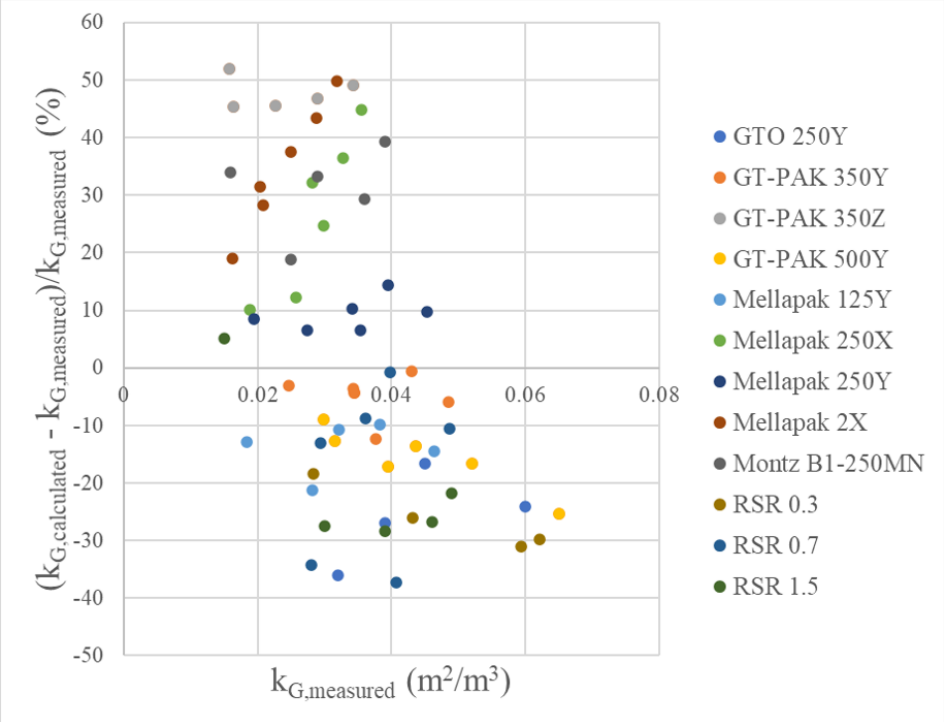

Figure 5.7: % error of k_G calculated by Equation 5.10 for all packings.

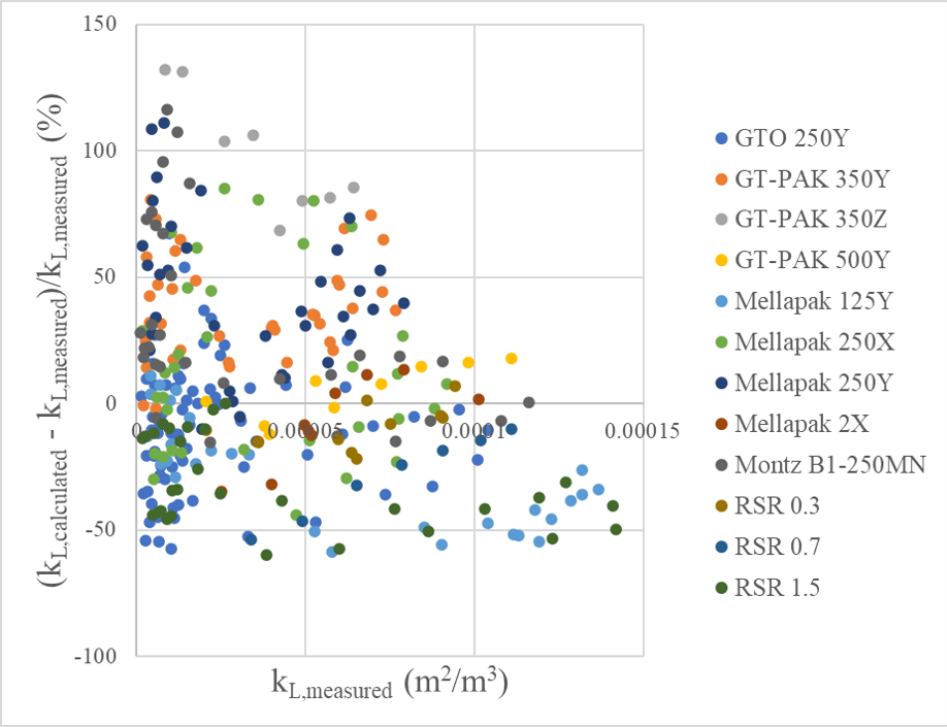

Figure 5.8: % error of k_L calculated by Equation 5.11 for all packings.

more poorly than that for a_e. However, this was not seen as a failure due to the fact that the magnitudes of k_G and k_L are much lower than that of a_e. In mass transfer models, k_G and k_L are always multiplied by a_e to calculate mass transfer flux. Therefore, accuracy in the prediction of a_e is much more important than accuracy in the prediction of k_G or k_L.

5.2 Mass Transfer Correlation Comparison

The mass transfer correlations developed in this work (Equations 5.4, 5.10, and 5.11) were compared with the literature correlations discussed in Chapter 2. In Figures 5.9 and 5.10, predictions for the correlations are plotted along with data for Mellapak 250Y and Raschig Super-Rings of size 1.5. The correlations developed in this work match the data much better in terms of both trend and magnitude than the literature correlations. Although the developed correlation for a_e bears strong resemblance to the Hanley and Chen correlation, the Hanley and Chen correlation has an inverse dependence on the liquid phase Reynolds number, which is the opposite of the trend ex-

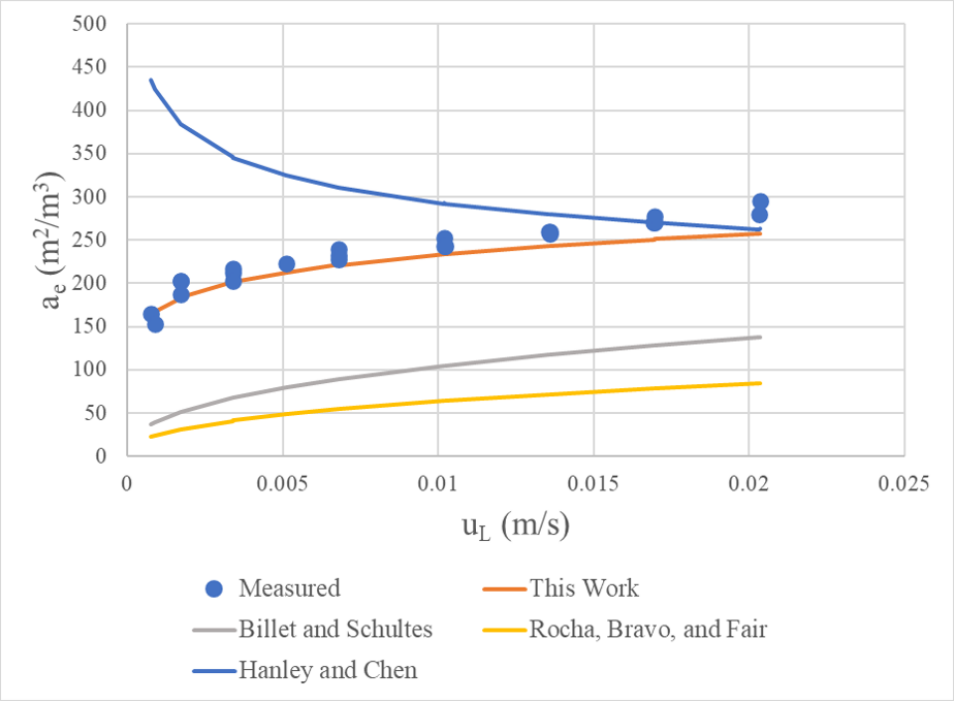

Figure 5.9: Predictions of Mellapak 250Y effective interfacial mass transfer area from correlations for structured packing.

pressed by the data. Tables 5.2-5.4 give a more broad overview of how the correlations developed in this work match the data compared to those from literature and further confirm the superior fit of the correlations developed in this work.

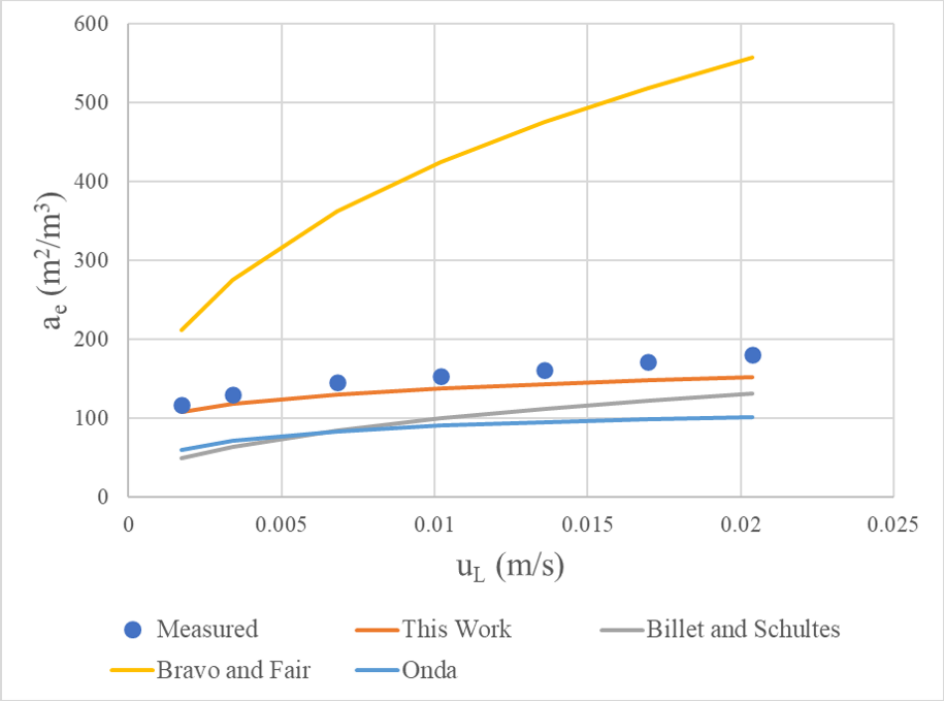

Figure 5.10: Predictions of Raschig Super-Rings 1.5 effective interfacial mass transfer area from correlations for random packing.

a_e Correlation	Mean % Error	Maximum % Error	Minimum % Error
Onda	-37.8	25.6	-78.1
Bravo and Fair	251	893	8.33
Billet and Schultes	21.9	1658	-88.4
Rocha, Bravo, and Fair	188	6110	-92.0
Hanley and Chen	59.9	983	-96.0
This Work	0.825	64.6	-35.7

Table 5.2: % error of a_e calculated by correlations.

k_G Correlation	Mean % Error	Maximum % Error	Minimum % Error
Onda	8.79	61.4	-19.7
Billet and Schultes	62.0	151	-25.7
Rocha, Bravo, and Fair	-31.0	-0.704	-58.3
Hanley and Chen	-81.6	-63.7	-90.8
This Work	3.20	51.8	-37.3

Table 5.3: % error of k_G calculated by correlations.

k_L Correlation	Mean % Error	Maximum % Error	Minimum % Error
Onda	40.3	233	-71.4
Billet and Schultes	202	831	-46.3
Rocha, Bravo, and Fair	230	1135	0.112
Hanley and Chen	-61.7	12.5	-97.6
This Work	7.14	132	-59.9

Table 5.4: % error of k_L calculated by correlations.

5.3 Design and Economic Analysis

Equations 5.4, 5.10, and 5.11 were implemented in ProMax as "User Defined" mass transfer correlations (as discussed in Chapter 4) and used to test seven random and structured packings in the ProMax CO_2 absorber model. The results are shown in Tables 5.5-5.6. For all of the packings tested, multiple absorber columns were required. This was due to the high flow rate of flue gas. To keep fraction flooding below 70% in these circumstances, the diameter of each column had to be large. When simulated as a single column, the absorber diameter calculated by ProMax was greater than the required absorber height. This is an impractical design, so multiple columns in parallel were instead assumed [Towler and Sinnott, 2013].

Raschig Super-Rings of size 1.5 are considered to be the optimum packing choice based on this analysis. Despite the lower pressure drop and, in turn, blower purchase and utility costs associated with the structured packings, the purchase cost of the column dominated the annualized cost, making the random packings generally more cost-effective than the structured packings.

Packing	# of Absorber Columns Required	Column Diameter (m)	Column Height (m)	Column Pressure Drop (kPa)	Blower Power (kW)
RSR 0.3	4	4.2	5.02	2.337	269.3
RSR 0.7	2	5.3	5.70	2.107	243.0
RSR 1.5	2	4.8	6.25	1.810	208.9
Mellapak 125Y	2	4.7	8.54	1.005	116.2
Mellapak 250X	2	4.7	8.01	1.183	136.8
Mellapak 250Y	2	5.3	6.86	1.017	117.7
GT-PAK 500Y	4	4.7	5.18	1.105	127.8

Table 5.5: ProMax simulation results for each tested packing.

Packing	Column(s) Purchase Cost (k$)	Blower Purchase Cost (k$)	Blower Utility Cost (k$/yr)	Annualized Cost (k$/yr)
RSR 0.3	3406	310.0	168.1	911.2
RSR 0.7	2131	285.7	151.6	634.9
RSR 1.5	1628	253.6	130.3	506.7
Mellapak 125Y	3838	159.6	72.53	872.1
Mellapak 250X	4252	181.5	85.36	972.0
Mellapak 250Y	4613	161.1	73.42	1028
GT-PAK 500Y	7335	172.0	79.73	1581

Table 5.6: CO_2 absorption unit costs associated with each tested packing.

6. CONCLUSIONS

New correlations for the effective interfacial mass transfer area, gas phase mass transfer coefficient, and liquid phase mass transfer coefficient in a packed column were developed. The correlations were regressed using data published elsewhere for various types of random and structured packing encompassing ranges of gas and liquid superficial velocities, liquid viscosity, and surface tension. The correlation for effective interfacial mass transfer area was developed with the capacity to account for trends with respect to these parameters as well as several packing-specific parameters, such as specific area, void fraction, material of construction, and corrugation angle in structured packing. Overall, the correlations fit the data well, with accuracy in predicting the magnitude and trends of data points exceeding that of literature correlations.

The new correlations were applied to modeling CO_2 capture by incorporating them into the process simulator ProMax and using ProMax to simulate a CO_2 absorber column treating flue gas from a 50MW coal-fired power plant. This study demonstrated use of the ProMax "User Defined" mass transfer correlation feature, which can be used to customize the software's mass and heat transfer column models. Multiple packings were tested in the absorber, and an economic analysis was used to determine that Raschig Super-Rings of size 1.5 were the optimal choice of packing under the specified conditions.

Future work relevant to this study includes testing the correlations with additional data and increasing the complexity of the CO_2 absorber case study. The correlations developed in this work are purely empirical and therefore may be significantly inaccurate outside of tested data regions. Furthermore, the data did not include any systematic variation of the physical properties of the gas phase, which makes dependencies on these variables in the correlation unsubstantiated. In terms of the CO_2 absorber case study, the economic analysis could be made more rigorous. Including factors like capital depreciation could change the relative importance of utility versus capital costs, which could change the conclusion of the study. Either of these measures would further this work's goal of developing and applying useful mass transfer correlations for CO_2 capture modeling.

REFERENCES

[EPA, 2018] (2018). Sources of greenhouse gas emissions. https://www.epa.gov/ghgemissions/sources-greenhouse-gas-emissions.

[BRE, 2020a] (2020a). *BRE-231: Sour Gas Processing: An Advanced Course on Removing Undesirable Components from Gases and Liquids*. Bryan Research and Engineering, LLC.

[EIA, 2020] (2020). Energy and the environment explained. https://www.eia.gov/energyexplained/energy-and-the-environment.

[BRE, 2020b] (2020b). *ProMax Help v5.0*. Bryan Research and Engineering, LLC.

[Aboudheir and McIntyre, 2009] Aboudheir, A. and McIntyre, G. (2009). Industrial design and optimization of CO_2 capture, dehydration, and compression facilities. Technical report, Bryan Research and Engineering, Inc.

[Billet and Schultes, 1993] Billet, R. and Schultes, M. (1993). Predicting mass transfer in packed columns. *Chemical Engineering Technology*, 16(1):1–9.

[Billet and Schultes, 1999] Billet, R. and Schultes, M. (1999). Prediction of mass transfer columns with dumped and arranged packings: Updated summary of the calculation method of billet and schultes. *Chemical Engineering Research and Design*, 77(1):498–504.

[Bravo and Fair, 1982] Bravo, J. L. and Fair, J. R. (1982). Generalized correlation for mass transfer in packed distillation columns. *Industrial and Engineering Chemistry Process Design and Development*, 21(1):162–170.

[CEPCI, 2009] CEPCI (2009). Economic indicators. *Chemical Engineering*, 116(2):64.

[CEPCI, 2020] CEPCI (2020). Economic indicators. *Chemical Engineering*, 127(9):72.

[Green and Perry, 2008] Green, D. W. and Perry, R. H. (2008). *Perry's Chemical Engineers' Handbook, 8th Edition*. McGraw-Hill Professional.

[Hanley and Chen, 2012] Hanley, B. and Chen, C.-C. (2012). New mass-transfer correlations for packed towers. *AIChE Journal*, 58(1):132–152.

[Incropera et al., 2007] Incropera, F. P., DeWitt, D. P., Bergman, T. L., and Lavine, A. S. (2007). *Fundamentals of Heat and Mass Transfer, 6th Edition*. Wiley.

[Kister, 1992] Kister, H. Z. (1992). *Distillation Design*. McGraw-Hill Education.

[Olujic et al., 2001] Olujic, Z., Jansen, H., Kaibel, B., Rietfort, T., and Zich, E. (2001). Stretching the capacity of structured packings. *Industrial and Engineering Chemistry Research*, 40(26):6172–6180.

[Onda et al., 1968] Onda, K., Takeuchi, H., and Okumoto, Y. (1968). Mass transfer coefficients between gas and liquid phases in packed columns. *Journal of Chemical Engineering of Japan*, 1(1):56–62.

[Rao and Rubin, 2002] Rao, A. B. and Rubin, E. S. (2002). A technical, economic, and environmental assessment of amine-based CO_2 capture technology for power plant greenhouse gas control. *Environmental Science and Technology*, 36(20):4467–4475.

[Rocha et al., 1993] Rocha, J. A., Bravo, J. L., and Fair, J. R. (1993). Distillation columns containing structured packings: A comprehensive model for their performance. 1. hydraulic models. *Industrial and Engineering Chemistry Research*, 32(4):641–651.

[Rocha et al., 1996] Rocha, J. A., Bravo, J. L., and Fair, J. R. (1996). Distillation columns containing structured packings: A comprehensive model for their performance. 2. mass-transfer model. *Industrial and Engineering Chemistry Research*, 35(5):641–651.

[Seider et al., 2008] Seider, W., Seader, J., Lewin, D., and Widagdo, S. (2008). *Product and Process Design Principles: Synthesis, Analysis, and Evaluation, 3rd Edition*. Wiley.

[Skowlund et al., 2012] Skowlund, C., Hlavinka, M., Lopez, M., and Fitz, C. (2012). Comparison of ideal stage and mass transfer models for separation processes with and without chemical reactions. Technical report, Bryan Research and Engineering, Inc.

[Song, 2017] Song, D. (2017). *Effect of Liquid Viscosity on Liquid Film Mass Transfer for Packings*. PhD thesis, University of Texas at Austin.

[Towler and Sinnott, 2013] Towler, G. and Sinnott, R. (2013). *Chemical Engineering Design: Principles, Practice and Economics of Plant and Process Design, 2nd Edition*. Butterworth-Heinemann.

[Tsai, 2010] Tsai, R. (2010). *Mass Transfer Area of Structured Packing*. PhD thesis, University of Texas at Austin.

[Wang, 2015] Wang, C. (2015). *Mass Transfer Coefficients and Effective Area of Packing*. PhD thesis, University of Texas at Austin.

[Wang et al., 2016] Wang, C., Song, D., Seibert, F., and Rochelle, G. (2016). Dimensionless models for predicting the effective area, liquid-film, and gas-film mass-transfer coefficients of packing. *Industrial and Engineering Chemistry Research*, 55(18):5373–5384.

[Wilson, 2004] Wilson, I. (2004). Gas-liquid contact area of random and structured packing. Master's thesis, University of Texas at Austin.

APPENDIX A

USER DEFINED MASS TRANSFER CORRELATION CODE

```
using System;
using ProMax = BRE.ProMax.Interop;
using PMXExtensibility = BRE.ProMax.Extensibility;

namespace CSCLR_RandomPacking_UDMTC
{
    public class CSCLR_UserDefinedMTC :
    PMXExtensibility.UserDefinedMassTransfer,
    PMXExtensibility.PersistStreamInit,
    IDisposable
    {
    private ProMax._StagedColumn m_StagedColumn;
    private double m_lfap; //Surface area per unit Volume (m^-1)
    private double m_lfVoidFrac; //Void fraction
    private double m_lfMatFac; //Material factor
    private double m_lfCorrAngle; //Corrugation angle (ř)
    private double m_lfPi, m_lfGravity;
    private int m_nComps;
    private bool m_bDirty;
    private bool m_bDisposed = false;

    //PMXExtensibility.UserDefinedMassTransfer
    public void BulkCompositionFactor(ProMax._FlashData FlashDataV,
      ProMax._FlashData FlashDataL, ProMax._Stage Stage, double[] BCF)
    {
      throw new NotImplementedException();
    }
    public void Individual_HeatTransfer(ProMax._FlashData FlashDataV,
      ProMax._FlashData FlashDataL, double Tinterface,
      double TotalRate, double[] Yinterface, double[] Xinterface,
      double[] ComponentRates, ProMax._Stage Stage,
      ref double CoeffV, ref double CoeffL)
    {
      throw new NotImplementedException();
    }
    public void Individual_K(ProMax._FlashData FlashDataV,
      ProMax._FlashData FlashDataL, double Tinterface,
      double TotalRate, double[] Yinterface, double[] Xinterface,
      double[] ComponentRates, ProMax._Stage Stage,
      double[,] KV, double[,] KL, ref double Area)
    {
      //Get stage height
      ProMax.Properties stageProperties = Stage.HardwareProperties[
        ProMax.pmxStageHardwareTypesEnum.pmxStageHardwareRandomPacking];
      ProMax._PDouble pdblStageHeight = (ProMax._PDouble)stageProperties[
        ProMax.pmxRandomPackingPropEnum.pmxRandomPackingStageHeight];
```

```
double stageHeight = pdblStageHeight.SIValue;

//Get column diameter
ProMax.Properties stagePropertiesD = Stage.HardwareProperties[
  ProMax.pmxStageHardwareTypesEnum.pmxStageHardwareGeneral];
ProMax._PDouble _StageDiam = (ProMax._PDouble)stagePropertiesD[
  ProMax.pmxStageGeneralHardwarePropEnum.pmxStageDiameter];
double ColumnDiameter = _StageDiam.SIValue;

//Determine if structured packing or random packing
ProMax._PLong _StageType = (ProMax.PLong)stagePropertiesD[
  ProMax.pmxStageGeneralHardwarePropEnum.pmxStageHardwareType];
bool bStrucPack = _StageType.get_Value() == (int)
  ProMax.pmxStageHardwareTypesEnum.pmxStageHardwareStructuredPacking;

//Get superficial vapor phase mass velocity
double lfG = FlashDataV.Property[ProMax.pmxPhasePropEnum.
  pmxPhaseMassFlow] / (m_lfPi * 0.25 * ColumnDiameter *
  ColumnDiameter);

//Get vapor viscosity and density
double lfViscV = FlashDataV.Property[ProMax.pmxPhasePropEnum.
  pmxPhaseDynViscosity];
double lfDensV = FlashDataV.Property[ProMax.pmxPhasePropEnum.
  pmxPhaseMassDensity];

//Get superficial liquid phase mass velocity
double lfL = FlashDataL.Property[ProMax.pmxPhasePropEnum.
  pmxPhaseMassFlow] / (m_lfPi * 0.25 * ColumnDiameter *
  ColumnDiameter);

//Get liquid viscosity, density, and surface tension
double lfViscL = FlashDataL.Property[ProMax.pmxPhasePropEnum.
  pmxPhaseDynViscosity];
double lfDensL = FlashDataL.Property[ProMax.pmxPhasePropEnum.
  pmxPhaseMassDensity];
double lfSurTen = FlashDataL.Property[ProMax.pmxPhasePropEnum.
  pmxPhaseSurfaceTension];

//Hydraulic diameter
double lfdh = 4 * m_lfVoidFrac / m_lfap;

double lfReV = lfG * lfdh / lfViscV; //Vapor phase Reynolds number
double lfReL = lfL * lfdh/ lfViscL; //Liquid phase Reynolds number
double lfVelocity2 = lfL * lfL /
  lfDensL / lfDensL; //Superficial liquid phase velocity squared
double lfFrL = lfVelocity2 / (lfdh *
  m_lfGravity); //Liquid phase Froude number
double lfWeL = lfDensL * lfVelocity2 * lfdh /
  lfSurTen;// Liquid phase Weber number

//Fractional effective interfacial area
double lf_ae_ap = 0.346 * m_lfMatFac * Math.Pow(lfReV, 0.162) *
  Math.Pow(lfReL, 0.0156) * Math.Pow(lfWeL, 0.0709) *
```

```
  Math.Pow(lfFrL, -0.0104) * (bStrucPack ? Math.Pow(
  Math.Cos(m_lfCorrAngle) / Math.Cos(Math.PI / 4), -0.12) : 1.0);

//Mass transfer area
Area = m_lfap * (m_lfPi * 0.25 * ColumnDiameter *
  ColumnDiameter * stageHeight) * lf_ae_ap;

//Temperatures and pressures for both phases
double lfT_V = FlashDataV.Property[ProMax.pmxPhasePropEnum.
  pmxPhaseTemperature];
double lfP_V = FlashDataV.Property[ProMax.pmxPhasePropEnum.
  pmxPhasePressure];
double lfT_L = FlashDataL.Property[ProMax.pmxPhasePropEnum.
  pmxPhaseTemperature];
double lfP_L = FlashDataL.Property[ProMax.pmxPhasePropEnum.
  pmxPhasePressure];

//Physical Property calculation object for each phase
ProMax.PhysProp PhysProp_L = FlashDataL.Environment.PhysProp;
ProMax.PhysProp PhysProp_V = FlashDataV.Environment.PhysProp;

//Schmidt number declarations for both phases
double lfScV;
double lfScL;

//Sherwood number declarations for both phases
double lfShV;
double lfShL;

//Binary diffusion coefficient declarations for both phases
double lfDij_L;
double lfDij_V;

//Individual mass transfer coefficient declarations for both phases
double kij_V;
double kij_L;

//Binary diffusion coefficients and individual mass transfer
//coefficients are calculated for all component pairs in the
//nested for loop. KV_ and KL_ are the matrices storing individual
//mass transfer coefficients for vapor and liquid phases.
for (int i = 0; i < m_nComps; i++)
{
  for (int j = 0; j < m_nComps; j++)
  {
    int uStatus = (int)ProMax.pmxPropStatusValues.pmxPropStatusOK;
    if (i == j)
    {
      KV[i, j] = 0.0;
      KL[i, j] = 0.0;
    }
    else
    {
      //Binary diffusion coefficients calculated as a
```

```
        //function of phase, temperature, pressure, and components
        lfDij_V = PhysProp_V.CalcBinary(ProMax.pmxPhysPropEnum.
          pmxDiffusionCoeff, ProMax.pmxPhaseEnum.pmxVaporPhase,
          (int)ProMax.pmxPropMaskValues.pmxNullPropMask, uStatus,
          lfT_V, lfP_V, i, j);
        lfDij_L = PhysProp_L.CalcBinary(ProMax.pmxPhysPropEnum.
          pmxDiffusionCoeff, ProMax.pmxPhaseEnum.pmxLLiquidPhase,
          (int)ProMax.pmxPropMaskValues.pmxNullPropMask, uStatus,
          lfT_L, lfP_L, i, j);

        //If correlation returns negative value, set it to zero.
        bool bFail = (uStatus & (int)ProMax.pmxPropStatusValues.
          pmxPhysPropFailure) == (int)ProMax.pmxPropStatusValues.
          pmxPhysPropFailure;
        if ((lfDij_V < 0.0) || bFail || double.IsInfinity(lfDij_V) ||
          double.IsNaN(lfDij_V))
          lfDij_V = 0.0;
        if ((lfDij_L < 0.0) || bFail || double.IsInfinity(lfDij_L) ||
          double.IsNaN(lfDij_L))
          lfDij_L = 0.0;

        //Individual mass transfer coefficient as a function of
        //diffusion coefficients and other parameters
        lfScV = lfDij_V == 0.0 ? 0.0 : lfViscV / (lfDij_V * lfDensV);
        lfScL = lfDij_L == 0.0 ? 0.0 : lfViscL / (lfDij_L * lfDensL);
        lfShV = 0.416 * Math.Pow(lfReV, 0.63) *
          Math.Pow(lfScV, 1.0 / 3.0);
        lfShL = 0.984 * Math.Pow(lfReL, 0.742) * Math.Pow(lfScL, 0.457);
        kij_V = lfShV * lfDij_V / lfdh;
        kij_L = lfShL * lfDij_L / lfdh;

        KV[i, j] = kij_V;
        KL[i, j] = kij_L;
      }
    }
  }
}
public void InitBeforeCalculate(ProMax._FlashData FlashData)
{
  //Get packing-specific properties
  ProMax.Properties Properties = m_StagedColumn.InternalMassTransfer
    .Properties;
  ProMax._PDouble AperV = (ProMax._PDouble)Properties["AperV"];
  ProMax._PDouble VoidFrac = (ProMax._PDouble)Properties["VoidFrac"];
  ProMax._PDouble MatFac = (ProMax._PDouble)Properties["MatFac"];
  ProMax._PDouble CorrAngle = (ProMax._PDouble)Properties["CorrAngle"];

  m_lfap = AperV.SIValue;
  m_lfVoidFrac = VoidFrac.SIValue;
  m_lfMatFac = MatFac.SIValue;
  m_lfCorrAngle = CorrAngle.SIValue;

  //Get number of components
  m_nComps = FlashData.Environment.Components.Count;
```

```
  //Get universal constants
  m_lfPi = m_StagedColumn.Project.Constant[ProMax.pmxConstantsEnum.
    pmxPi].SIValue;
  m_lfGravity = m_StagedColumn.Project.Constant[ProMax.pmxConstantsEnum.
    pmxAccelGravity].SIValue;
}
public void InterfaceEquilibriumFactor(ProMax._FlashData FlashDataV,
  ProMax._FlashData FlashDataL, double Tinterface, double TotalRate,
  double[] Yinterface, double[] Xinterface, double[] ComponentRates,
  ProMax._Stage Stage, double[] IEF)
{
  throw new NotImplementedException();
}
public void Overall_HeatTransfer(ProMax._FlashData FlashDataV,
  ProMax._FlashData FlashDataL, ProMax._Stage Stage, ref double Coeff)
{
  throw new NotImplementedException();
}
public void Overall_K(ProMax._FlashData FlashDataV,
  ProMax._FlashData FlashDataL, ProMax._Stage Stage,
  double[,] K, ref double Area)
{
  throw new NotImplementedException();
}
public void SetOwner(ProMax._Block Owner)
{
  m_StagedColumn = (ProMax._StagedColumn)Owner;
}
public void InitNew()
{
  double AperV = 101.7060367; //Surface area per unit Volume (m^-1)
  double VoidFrac = 0.95; //Void fraction
  double MatFac = 1.0;  //Material factor
  double CorrAngle = Math.PI / 4; //Corrugation angle (rad)

  ProMax.PropertiesEx PropertiesEx = (ProMax.PropertiesEx)m_StagedColumn.
    InternalMassTransfer.Properties;
  ProMax.PDouble PDouble = new ProMax.PDouble();
  PDouble.Name = "AperV";
  PDouble.Label = "Surface Area / Volume";
  PDouble.UnitsEnum = ProMax.pmxUnitsEnum.pmxRecipLengthUnit;
  PDouble.SIValue = AperV;
  PropertiesEx.AddCopy(PDouble);

  PDouble.Name = "VoidFrac";
  PDouble.Label = "Void Fraction";
  PDouble.UnitsEnum = ProMax.pmxUnitsEnum.pmxDimensionlessUnit;
  PDouble.SIValue = VoidFrac;
  PropertiesEx.AddCopy(PDouble);

  PDouble.Name = "MatFac";
  PDouble.Label = "Material Factor";
  PDouble.UnitsEnum = ProMax.pmxUnitsEnum.pmxDimensionlessUnit;
```

```
      PDouble.SIValue = MatFac;
      PropertiesEx.AddCopy(PDouble);

      PDouble.Name = "CorrAngle";
      PDouble.Label = "Corrugation Angle";
      PDouble.UnitsEnum = ProMax.pmxUnitsEnum.pmxAngleUnit;
      PDouble.SIValue = CorrAngle;
      PropertiesEx.AddCopy(PDouble);

      m_bDirty = true;
    }

    //PMXExtensibility.PersistStreamInit
    public bool IsDirty()
    {
      return m_bDirty;
    }
    public void Load(System.Runtime.InteropServices.ComTypes.IStream pStm)
    {
      m_bDirty = false;
    }
    public void Save(System.Runtime.InteropServices.ComTypes.IStream pStm,
      bool fRemember)
    {
      m_bDirty = false;
    }

    //IDisposable
    public void Dispose()
    {
      if (m_bDisposed)
        return;
      m_bDisposed = true;
      if (m_StagedColumn != null)
        System.Runtime.InteropServices.Marshal.
          ReleaseComObject(m_StagedColumn);
    }
  }
}
```

APPENDIX B

ADDITIONS TO PROMAX COLUMNHARDWARE.XML FILE

```
<Hardware Name="Raschig Super-Rings 0.7 metal">
    <Label xml:lang="en">Raschig Super-Rings 0.7 metal</Label>
    <Label xml:lang="es">Empaque aleatorio definido por el usuario</Label>
    <Label xml:lang="zh-CN"></Label>
    <Item Name="pmxRandomPackingTypesEnum">pmxRandomPackUserDefined</Item>
      <Item Name="pmxPackingMaterialTypesEnum">pmxPackingMaterialMetal</Item>
      <Item Name="pmxRandomPackingFloodModelEnum">
   pmxRandomPackFloodModelBilletSchultes</Item>
      <Item Name="pmxRandomPackingSurfaceArea">180</Item>
      <Item Name="pmxRandomPackingVoidFraction">0.98</Item>
      <Item Name="Nominal Diameter">0.024</Item>
      <Item Name="Billet Cfl">2.2</Item>
      <Item Name="Billet Cp">0.668</Item>
      <Item Name="Billet Ch">0.672</Item>
      <Item Name="Billet CL">1.386</Item>
      <Item Name="Billet Cv">0.434</Item>
    </Hardware>
  <Hardware Name="Raschig Super-Rings 1.5 metal">
    <Label xml:lang="en">Raschig Super-Rings 1.5 metal</Label>
    <Label xml:lang="es">Empaque aleatorio definido por el usuario</Label>
    <Label xml:lang="zh-CN"></Label>
    <Item Name="pmxRandomPackingTypesEnum">pmxRandomPackUserDefined</Item>
      <Item Name="pmxPackingMaterialTypesEnum">pmxPackingMaterialMetal</Item>
      <Item Name="pmxRandomPackingFloodModelEnum">
   pmxRandomPackFloodModelBilletSchultes</Item>
      <Item Name="pmxRandomPackingSurfaceArea">120</Item>
      <Item Name="pmxRandomPackingVoidFraction">0.98</Item>
      <Item Name="Nominal Diameter">0.04</Item>
      <Item Name="Billet Cfl">2.148</Item>
      <Item Name="Billet Cp">0.482</Item>
      <Item Name="Billet Ch">0.735</Item>
      <Item Name="Billet CL">1.307</Item>
      <Item Name="Billet Cv">0.42</Item>
    </Hardware>
  <Hardware Name="GT-PAK 500Y">
    <Label xml:lang="en">GT-PAK 500Y</Label>
    <Label xml:lang="es">Empaque estructurado definido por el usuario</Label>
    <Label xml:lang="zh-CN"></Label>
    <Item Name="pmxStructuredPackingTypesEnum">pmxStructPackUserDefined</Item>
      <Item Name="pmxPackingMaterialTypesEnum">pmxPackingMaterialMetal</Item>
      <Item Name="pmxStructuredPackingFloodModelEnum">
   pmxStructuredPackFloodModelBilletSchultes</Item>
      <Item Name="pmxStructuredPackingSurfaceArea">500</Item>
      <Item Name="pmxStructuredPackingVoidFraction">0.95</Item>
      <Item Name="Billet Cfl">2.43</Item>
      <Item Name="Billet Cp">0.31</Item>
```

```
  <Item Name="Billet Ch">0.68</Item>
  <Item Name="Billet CL">1.354</Item>
  <Item Name="Billet Cv">0.515</Item>
  <Item Name="Corrugation Size">0.008</Item>
  <Item Name="Corrugation Angle">0.7853981633974480</Item> <!-- 45 Deg-->
</Hardware>
```